SYNTHESIS AND CHARACTERIZATION OF ZINC OXIDE NANOPARTICLES CONJUGATED WITH FERULIC ACID AND INVESTIGATION OF OPTICAL TRANSITION PROPERTIES OF FERULIC ACID USING SPECTROSCOPIC TECHNIQUES

By

YIRGA KASSA

A THESIS SUBMITTED IN PARTIAL FULFILMENT OF THE REQUIREMENT FOR THE DEGREE OF DOCTOR OF PHILOSOPHY IN PHYSICS (LASER SPECTROSCOPY)

AT

DEPARTMENT OF PHYSICS

ADDIS ABABA UNIVERSITY

ADDIS ABABA, ETHIOPIA

OCTOBER 2020

ADDIS ABABA UNIVERSITY
DEPARTMENT OF PHYSICS

The undersigned hereby certify that they have read and recommend to the Program of Graduate Studies for acceptance a thesis entitled "Synthesis and Characterization of Zinc Oxide Nanoparticles Conjugated With Ferulic Acid and Investigation of Optical Transition Properties of Ferulic Acid Using Spectroscopic Techniques" by Yirga Kassa in partial fulfillment of the requirements for the degree of doctor of philosophy in Physics.

Dated: 10/04/ 2020

External Examiner: _____
To be Assigned

Research Supervisor: _____
Late Professor Ashok Gholap, Dr. Belayneh Mesfin

Examing Committee: _____
To be Assigned

_____
To be Assigned

ADDIS ABABA UNIVERSITY

Date: 10/04/2020

Author: **Yirga Kassa**

Title: Synthesis and Characterization of Zinc Oxide Nanoparticles Conjugated With Ferulic Acid and Investigation of Optical Transition Properties of Ferulic Acid Using Spectroscopic Techniques.

Department: **Physics**

Degree: **Ph.D.** Convocation: October Year: **2020**

Permission is herewith granted to Addis Ababa University to circulate and to have copied for non-commercial purposes, at its discretion, the above title upon the request of individuals or institutions.

Signature of Author

Dedicated to

My Former Advisor Late Professor Ashok V. Gholap

Table of Contents

List of Tables

List of Figures

Abrivation

NPs: Nanoparticles

FA: Ferulic acid

ICDD; International Centre for Diffraction Data

ICSD: Inorganic Crystal Structure Database

FTIR: Fourier transform infrared

SEM: Scanning electron microscope

UV/Vis: Ultra violate viable

XRD: X-ray diffraction

CD: Circular dichroism

PL: Photoluminescence

JAZ 3 Chanel: Ocean optics spectrophotometer

FWHM: full width at half maximum

FA-ZnO NPs: Interaction of ferulic acid with zinc oxide nanoparticles

CA-ZnO NPs:Interaction of cafic acid with zinc oxide nanoparticles

CGA-ZnO NPs:Interaction of chlorogenic acid with zinc oxide nanoparticles

FRET: Fluorescence Resonance Energy Transfer

RET: Resonance Energy Transfer

UDM: Uniform deformation model

Abstract

In this research, synthesis and characterization of zinc oxide nanoparticle (ZnO NP), transition optical properties, self-association properties and the binding of ferulic acid (FA) and ZnO NPs are investigated. ZnO NP was synthesized by sol-gel synthesis approach and its optical, structural properties and its purity were investigated using spectroscopic and microscopic techniques. Equal association constant (EK) dimer model, fluorescence quenching method, the Stern-Volmer equation (model) and Van't Hoff equation were utilized for analyzing and interpreting data.

Our finding revealed that the synthesized ZnO NPs exhibits hexagonal wurtzite structure with lattice parameters $a = 0.3250677\ nm$ and $c = 0.5212783\ nm$. It has average grain size and band gap energy are 19.89 nm and 3.29 eV, respectively. It's surface consists of O-H stretching, C-O-H bending, C-O stretching, O-H bending and Zn-O stretching vibration. The mechanism of quenching is static quenching. Bimolecular binding constant decreases as temperature increases. Consequently, the fluorescence quenching was initiated by the formation of non-fluorescent FA-ZnO NP complex. Enthalpy and entropy changes were found to be $-53.301\ kJ/mol$ and $-76.27\ J/Kmol$. Accordingly, Van der Waals and hydrogen bond forces play a major role in FA and ZnO NP interaction. The efficiency of energy transfer between FA and ZnO NP was obtained to be 52.31%. Increasing FA concentration causes the molecules to aggregate and to shift the absorbance maxima. The enthalpy and entropy changes were obtained to 10.703 kJ/mol and 110.02 $(J/Kmol)$, respectively at all temperatures and Gibbs free energy at the temperatures 298 K, 310 K and 320 K were -22.084, -23.405 and -24.505 (KJ/mol), respectively.

Acknowledgements

Above all, I would like to thank the Almighty God, who offered me everything.
I would like to express my special appreciation and thanks to my advisors Professor Ashok Gholap and Dr. Belayneh Mesfin.
Dr.Belayneh Mesfin, Your advising is indispensable because you did these within short and tight time.
I would like to express my respect and appreciation from the heart to Dr. Teshome Senbeta for his facilitation and guidance. Especially, he facilitated my internship process. He directed me what I have to do while I lost my former advisor, Ashok Gholap.
Special thanks go to graduate program of AAUb and Debre Tabor University.
I would like to express the deepest appreciation CEITEC Nano Research Infrastructure (ID LM2015041, MEYS CR, 20162019), CEITEC Brno University of Technology. More of the experimental parts of this work were carried out with support of CEITEC Nano Research Infrastructure. I am deeply grateful to Dr. Michal Urbnek, (head of CEITEC Nano), Richard Kol (CEITEC Nano RI Manager), Dr.Zita, Dr.Flip with their colleagues for giving me free access the laboratory facilities, technical assistances and trainings.
I would also like to thank my parents and my beloved wife, Yeshiwork Abebaw for supporting me and encouraging me.

Chapter 1

1 Introduction

1.1 Spectroscopy

Spectroscopy deals with the interactions that exist between electromagnetic radiation and matter [1]. It includes the interactions of light with atoms and molecules in order to exploit physical and chemical properties of matter. The experimental spectroscopic data that provides the frequency or wavelength of the radiation and amount of radiation emitted, absorbed, reflected or scattered by the sample of molecules that give the information which enabled us to determine the quantitative and qualitative values of various molecular properties. This includes size, shape, flexibility, electronic arrangements and purity of atoms and molecules. Moreover, from the experimental spectroscopic data, we can estimate the tendency of self and hetro-association of atoms and molecules [2, 3].

In fact, most of our knowledge about matter is based on spectroscopic investigations. The experimental investigations of the composition and structure of atoms and molecules are accompanied with theoretical concepts. As a result, working principles, efficiencies, speeds and accuracy of spectrophotometers are nurtured through

time. Likewise, the scope of the application of spectroscopy is grown up. The foundations of molecular spectroscopy were laid at the beginning of nineteenth century. This field was exploded following the invention of laser in the 1960s equipped with a monochromatic, intense and tunable light source [4, 5]. A further step was taken in the 1980s, when laser spectroscopy emerged from the universities as an analytical discipline in an investigation of atomic and molecular information with increasingly commercial applications in physics, nanotechnology, chemistry, pharmacy, medicine, geology, biology and engineering. High resolution spectroscopy was rapidly developed associated with the spectra study of atoms and molecules in general, and to assess the information associated with the properties of matter. Most of the spectroscopic methods are based upon the principles of absorption, emission, fluorescence, ionization or scattering [6]. Varieties of spectroscopic techniques are regularly applied to solid, liquid and gaseous samples. The absorption and fluorescence spectroscopies are widely used spectroscopic methods. Moreover, these techniques are the most useful techniques that have various applications to study the rate of chemical reaction, molecular interactions, and the solvent, concentration and the temperature effect on the molecules and nanoparticles (NPs) optical and structural properties.

The self-association of small organic molecules to form large clusters gets a large interest in chemistry, physics and biology. In nature, predominantly in living systems, self-association of molecules plays a very vital role. Self-association of bioactive molecules that are driven noncovalent intermolecular interactions is a convenient means for the manufacturing of new functional materials. Pharmacologically active compounds can display amphiphilic properties due to there will be molecular aggregation in solution [7]. The aggregate formation can play a significant role in the

biological function of a molecule because it can control the passage of the molecules through membranes. These in turn change diffusion speed and modification of the interactions with other molecules [7]. The potential of aggregated and unaggregated drugs to pass throughout a membrane are the vital means for quantifying the biological functions of bioactive molecules [8].

Colloidal ZnO particle is one of those nanoparticles, which have extensive applications in molecular diagnostics, bioengineering, drug delivery systems and bimolecular imaging. The conjugation of colloidal ZnO particles with bioactive compounds enhances the physiochemical properties of particles due to the introduction of functional groups on the surface of nanoparticles. Ferulic acid is a family of phenolic compounds that has low toxicity and possesses many physiological functions, such as antimicrobial, anticancer (for instance lung, breast and skin cancer), anti-inflammatory, anti-arrhythmic, anti-diabetic and antithrombotic activities, and immune-stimulant properties. It has been widely used in food preservation and as additives in pharmaceutical products.

When ligand bounds to nanoparticles surface, it controls the growth of particles during synthesis, stabilizes the particles and prevents the aggregation of the nanoparticles [9, 10]. The ligand molecules bound to the surface of particles by some attraction either chemisorptions, electrostatic, hydrophobic and hydrogen bonds and Van der Waals forces [11]. Colloidal ZnO particles, which are conjugated with ligands, have extensive applications in molecular diagnostics, bioengineering, and bimolecular imaging [12, 13]. The conjugation of biomolecules with nanoparticles also introduces biocompatible functionalities into these nanoclusters and leads to the stabilization of the complex.

Many studies have been recently reported on the interaction of ZnO NPs with natural organic matter, and the results indicated the physicochemical properties of particles are changed due to the introduction of functional groups on the surface of ZnO NPs [13, 14]. The study conducted on the interaction of ZnO NPs with formic acid showed the adsorption of formic acid on the surface of ZnO NPs and a broad photoluminescence (PL) emission of the particle after the sample exposed to HCOOH, which is attributed to an exciton trapped by the surface format of the species. Similarly, ZnO NPs with folic acid interaction study also showed the growth of ZnO NPs in the presence of the natural compound, folic acid, exhibited interesting structural and bandgap properties [12]. Likewise the study conducted on the binding of zinc oxide nanoparticles with caffeic acid (CA) and chlorogenic acid (CGA) confirmed that the CA-ZnO NPs and CGA-ZnO NPs complex were formed that decrease the fluorescence intensity. These studies were carried out by using commercial zinc oxide nanoparticles [15].

A wide range of photophysical techniques, such as UV-Vis absorbance, fluorescence spectroscopy, FTIR spectroscopy, X-ray diffraction (XRD) and scanning electron microscopy (SEM), have been developed to characterize various aspects of the natural organic matters particularly their interactions with ZnO NP.

Detail of fluorescence spectral analysis such as binding constants, the binding sites, thermodynamic parameters and the efficiency of energy transfer between organic molecules and NPs are not investigated well.

In general, previously many authors have reported on the impact of the interactions

nanoparticles with phenolic compounds (bioactive molecules) which have various applications in the pharmaceutics, foodstuff and cosmetics [16, 17]. Moreover, the interaction of drug compounds with other drugs and foodstuff components may affect the pharmacodynamics and pharmacokinetics of the drugs [18]. Thus, the probing of the interactions nanoparticles with drug compounds, self interactions of drug compound and the interaction of drug compounds with food supplements is vital for the development of new types of drugs, to enhance their physiological activities and design more advanced and controllable carriers of drugs and food components [16, 18].

In this research, the synthesis of zinc oxide nanoparticles was carried out by the sol-gel method from zinc acetate and sodium hydroxide and its optical and structural properties are investigated by spectroscopic techniques. The conjugation of nanoparticles with bioactive compounds enhances the physiological functions of both the nanoparticles and the bioactive compounds. As a result, the binding of the zinc oxide nanoparticles with ferulic acid was investigated by fluorescence quenching method. We used circular dichroism (CD) J-1500, Jasco spectrophotometer to measure the emission of our samples. The measurement was taken at three different temperatures. From fluorescence quenching spectra analysis, the binding constants, the binding sites, thermodynamic parameters, the binding force operating between the compounds has been investigated using Vant Hoff equation. Moreover, the efficiency of energy transfers and distance between the donor (FA) and acceptor (ZnO PNs) were calculated in accordance to the Foresters no radiate energy transfer theory. Circular Dichroism spectroscopic technique was used for measuring the intensity of absorption of light. The study is concerned with the investigation of self-association, optical transition probability and thermodynamic parameters of ferulic acid because

these properties are not yet investigated in this regard.

1.2 Objectives of the Study

This research was initiated with following general and specific objectives.

1.2.1 General Objective

The general objective of the dissertation is to explore the optical and structural properties of zinc oxide nanoparticles, optical transition properties of ferulic acid, the binding properties of zinc oxide nanoparticle and ferulic acid.

1.2.2 Specific Objectives

This research consists of the following specific objectives:

1. To synthesize zinc oxide nanoparticle with sol-gel method.

2. To characterize the optical and structural properties of zinc oxide nanoparticles using spectroscopic techniques.

3. To probe the self-association of ferulic acid.

4. To study the optical transition properties of ferulic acid

5. To investigate the binding of zinc oxide nanoparticles with ferulic acid by fluorescence quenching approach.

1.3 Organization of the Thesis

This dissertation is organized as follows:

Chapter 1: This Chapter deals with the general overview of spectroscopy, types of spectroscopic techniques, applications of spectroscopy, the highlight of the binding of colloidal nanoparticles with bioactive compounds are included. General and specific

objectives of the study and the overall structure of the dissertation are also presented under this Chapter.

Chapter 2: It consists of literature reviews that concern on the general view of nanotechnology, the highlight of nanoascience, and nanomaterials, properties and nanomaterials applications, structural and optical properties of zinc oxide nanoparticle, reviews on some applications of zinc oxide nanoparticles, physiochemical properties and physiological functions of ferulic acid.

Chapter 3: Under this Chapter theories related to the derivation of electromagnetic wave equation from Maxwell's equations and the quantum mechanical derivation that is often used for qualitative and quantitative understanding of how transitions are induced in molecular system when it interacts with electromagnetic radiation are presented. The Schrodingers equation is introduced and simple problems to illustrate its relation to quantities that are important in molecular spectroscopy are solved. Fluorescence quenching mechanisms, types of fluorescence quenching, factors of fluorescence quenching, fluorescence resonance energy transfer are discussed.

Chapter 4: Chapter four explains the materials and methods used in this work. Here the methods of synthesis, characterization, binding study, dimerization study and optical transition properties of ferulic acid are discussed.

Chapter 5: Results and Discussion. Under this Chapter, the results of study are presented and discussed. The structural and optical properties of zinc oxide nanoparticles are illustrated. The binding of zinc oxide nanoparticles and ferulic acid is described. The chemo physical properties of ferulic acid are discussed.

Chapter 6: Finally, the conclusion and recommendation of the study is presented.

Chapter 2

Literature Review

2.1 Nanomaterials and Nanotechnology

Nanomaterials are intentionally man made materials at least one of their dimension is below 100 nm and have different physiochemical properties from the corresponding bulk materials. Moreover, their properties are size dependent [19]. This includes the optical, magnetic, electrical, and structural properties of nanomaterials that acquired the scientists' and engineers' attention. These interesting properties have great potential, for nanomaterials to have a significant impact on electronics, medicine, agriculture, industries and other fields [20].

Nanotechnology is the ability of designing, characterizing, producing and utilizing the materials, structures, systems and devices in nanoscale (1-100 nm) dimension by controlling their shape and size [21, 22]. It involves research conducting and technology development at atomic and molecular levels to create and use structures, devices and systems with fundamentally new molecular organizations that have novel properties and functions [23].

The term nanoscience was defined at the Royal Society London in 2004, as "Nanoscience

is the study of structures and manipulation of materials at nanoscale where properties of the nanomaterials differ significantly from their corresponding bulk." It deals with the fundamental relationships between physical properties and phenomena in the nanometer scale [24].

2.2 Zinc Oxide Nanoparticles

Zinc oxide (ZnO) nanoparticles are a symbol of a vital class of commercially applied materials. They have been widely applied for diagnostics, therapeutics, drug-delivery systems [25], cosmetics, personal care products, and food additives, due to their catalytic, semiconducting, antimicrobial, ultraviolet protective, and binding properties [26]. ZnO nanoparticles have received extensive applications in electronic and optoelectronic devices due to their exceptional electrical and optical properties [27]. They have been used in many practical applications such as solar cells [28], UV light-emitting devices, gas sensors [20], and photocatalysis [29].

Furthermore, they have also great potential in biological applications largely due to increases in surface area to volume ratio and quantum effects, which can affect the chemical reactivity and other physical and chemical properties. The similarity in the dimension of nanoparticles and biomolecules is another feature that makes them for biological applications [28]. Their nanoscale size helps them to internalize into cells and allow them to interact with biomolecules within or on the cell surface [30]. The electrostatic nature of nanoparticles is another important consideration that plays an important role in cellular adhesion and uptake [24].

ZnO nanoparticles can be synthesized in a number of ways. Among those sol-gel method is a popular method because it is a low cost, reproducible, reliable, simple

and relatively soft conditions of synthesis. In addition, nanoparticles produced by this method, show good optical properties, and the morphology of particles can be tailored by controlling the relative rate of hydrolysis and condensation reactions. However, it can be difficult to control these reaction rates.

2.2.1 Structural Properties of Zinc Oxide Nanoparticles

Zinc oxide is an inorganic semiconductor binary compound with the molecular formula ZnO. It is intrinsically n-type semiconductor nanoparticle that appears as a white powder. Naturally, it occurs in crystalline form in the mineral of zincite. The common crystal structures of ZnO are wurtzite B_4, zinc blende B_3, and rock salt B_1, as schematically shown in Fig. 1. Zinc blende zinc oxide nanoparticle structure is stabilized only due to the growth the cubic substrates and the rock salt structure can be obtained at relatively high pressures. At ambient conditions, thermodynamically stable phase is wurtzite. This belongs to the space group P63mc and has hexagonal unit cell with lattice parameters a = 0.3296 nm and c = 0.52065 nm. In wurtzite hexagonal structure, each anion, O^{2-} is encircled by four cations, Zn^{2+} at the corners of the tetrahedron, which shows the tetrahedral coordination. It has a considerable ionic character, which resides at the borderline between covalent and ionic semiconductor [31].

2.2.2 Optical Properties of Zinc Oxide Nanoparticles

ZnO is a wide band gap semiconductor. It exhibits large optical transparency and luminescent properties in the visible and near-ultraviolet regions [32]. Most literatures display that the band gap of zinc oxide nanoparticles at low and room temperatures are 3.44 eV and 3.37 eV, respectively. Because of these properties, ZnO nanoparticle

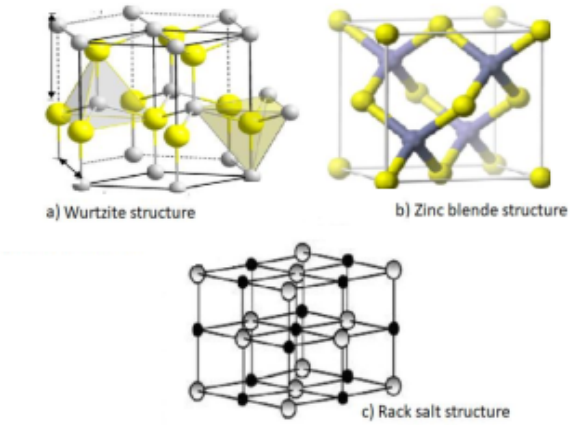

Figure 2.1: Crystal structures of zinc oxide nanoparticle.

has various applications for instance, it is used widely in electronic and optoelectronic applications such as solar cells, UV detectors and emitters, light-emitting diodes, laser diodes, photo-detectors and gas sensors [31]. Zinc oxide nanoparticle possesses high exciton binding energy which is 60 meV) that enables it to be more applicable for excitonic transitions even at room temperature. This implies that zinc oxide nanoparticle has high radiative recombination efficiency for spontaneous emission. Because of this zinc oxide nanoparticle is the most gifted material for optical devices, which are based on excitonic effects. Moreover, it has a lower threshold voltage for laser emission. Zinc oxide nanoparticle has strong luminescence in the green-white region of the spectrum. Due to this, it is vastly used for phosphor applications and due to its n-type conductivity, it is more promising material for the applications. For instance, it is more appropriate in vacuum fluorescent displays and field emission displays. Of course, the source of its luminescence center and luminescence mechanism is not certainly understood. Although many recent studies debated that the zinc vacancy is

a major cause for luminescence center and luminescence mechanism, none of them cannot provide strong argument which can be taken as a strong evidence [33].

The low symmetricity of the wurtzite hexagonal structure and the large electromechanical coupling properties of zinc oxide nanoparticle render it to have strong piezoelectric and pyroelectric properties, which are usually used for the applications such as sensors, transducers and actuators. On the other hand, high piezoelectric and pyroelectric can be described as the ability of generating the temporary voltage when they are heated or cooled. As a result, the temperature change adjusts the locations of the atoms slightly inside the crystal structure, such that the polarization of the material changes [34].

The conductivity of ZnO NPs is very sensitivity and when it is exposed to various gases, it used to detect them. Therefore, it is used to detect various gases and the freshness of foods and drinks with less cost. Few decades ago, the mechanisms of sensor action were not deeply investigated [35].

Recent experiments disclose the presence of a surface electron accumulation layer in vacuum galvanized single crystals, which vanishes when it is exposed to ambient air. This layer can also be used for a sensor action, as well. The existence of this conducting surface channel has been proposed to be associated to some confusing type-conversion properties observed when trying to attain p-type ZnO. On the other hand, the high thermal conductivity property of zinc oxide nanoparticle is used for various applications. For instance it is used as an additive to rubber for the purpose of enhancing the conductivity of the tires.

Zinc oxide nanoparticle device manufacturing processes prominently benefit from the amenability to low-temperature wet chemical design. Many authors reported that

those ZnO thin films could be designed with, alkaline, acidic as well as mixture solutions. This possibility of low-temperature chemical engraving improves its flexibility greatly in the processing, manipulative and integration of optoelectronic and electronic devices.

2.3 Ferulic Acid (FA)

Ferulic acid $C_{10}H_{1O}O_4$ is the most plentiful, omnipresent hydroxyl cinnamic acid derived from physiochemical phenolic acids, dispersed widely throughout the plant kingdom (spices, vegetables, grains, pulses, legumes, cereals, and fruits) in the form as ester or glycosides, lignin components, and hydrolysis tannins, in medicinal plants and also in their by-products (tea, cider oil, and beverages) [36]. Furthermore, FA can be produced by chemical synthesis and through biological transformation [36].

Ferulic acid (FA) is considered as an integral part of diet because it is widely distributed through spices, vegetables, grains, pulses, legumes, cereals, and fruits, their by-products (tea, cider oil, and beverages) [37]. It is absorbed and easily metabolized in the human body and stays in the blood for a long time.

It has been reported that FA has various physiological functions, including antioxidant, antimicrobial, antibacterial, antiinflammatory, anti-thrombosis, anti-allergic, hepatoprotective, antiviral, anticarcinogenic and antidiabatic [36]. It defends against coronary disease, reduces cholesterol, and enhances sperm viability.

Besides to this, it is used as a precursor for producing vanillin, and as a renewable resource to convert chemicals into other valuable aromatic chemicals from agricultural by-products in nature [38, 39]. it has been widely used in pharmaceutics and food preservation. Ferulic acid is a free radical scavenger but also inhibits enzymes that

catalyze free radical generation and enhances the scavenger enzyme activity. Because of its ability to neutralize free radicals in muscle tissue (alleviate muscle fatigue), it is used as a sports supplement. Furthermore, it decreases nerve cell damage and helps to repair damaged cells. Ferulic acid has the ability to absorb the UV long wavelength. As a result, it helps to protect the human body from UV radiation. So that it is widely applied in the cosmetics industry to produce the skincare formulations as a photoprotective agent (sunscreens), delayer of skin photoaging processes, however, its use is limited by its tendency to be rapidly oxidized [36]. Owing to the antioxidant and cholesterol-lowering activities, as well as the preventive effects against thrombosis and atherosclerosis, FA is considered a potential chemopreventive agent against coronary heart disease [38] (FA) (4-hydroxy-3-methoxy cinnamic acid) (Fig. 2.2) possesses three distinct structural motifs that can perhaps contribute to the free radical scavenging potential. The occurrence of electron-donating groups on

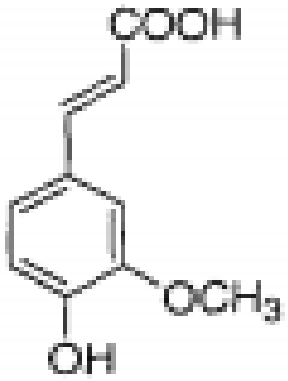

Figure 2.2: Molecular structure of Ferulic Acid.

the benzene formula (3 methoxy and 4-hydroxyl) of FA gives the extra property cease the radical chain reactions and the carboxylic acid group acts as an anchor of FA, by

which it binds to biomolecules such as lipids and proteins to modify their structural properties and altering their biological functions.

Moreover, many authors devoted a considerable interest in the interactions of phenolic compounds with nanoparticles [9, 40]. Because of these properties and its low toxicity, ferulic acid is now widely used in the food and ornamental industries [40, 41].

Chapter 3

Interaction of Ligth With Matter

Light-matter interaction has indispensable information to study the physical and chemical properties of matter. Ligth matter interaction can be described either classicaly or quantum mechanically. In classical aspect, lightmatter interactions are taken as a result the interactions of charged particles of the matter and a resonantly oscillating electromagnetic field. In this case , either by light-induced changes to the matter, such as ionization and photochemistry or changes to the light induced by the matter, such as absorption or emission of new light fields. Quantum mechanically, light-matter interaction will be considered as a perturbation induced by the light, which acts on the matter. This process is accompanied with stimulated emission, absorption and spontaneous emission. In this chapter the interaction of light with matter is discussed classically and semi-classically. The Maxwells equations and the wave equations are reviewed. Applying the classical electromagnetic theory, the optical phenomena that can be carried out in medium such as absorption and dispersion of the light are discussed. Moreover, the mathematical derivation that are used in quantitative and qualitative analysis about the transitions induced in molecular system are explained by semi-classical approach.

3.1 Maxwells Equations and the Wave Equations

The phenomena of electromagnetic radiation is a combination of an electric and magnetic fields that oscillate in phase being mutually perpendicular to each other. Both the electric and magnetic fields are also perpendicular to the direction of the propagation of the radiation. A moving charge (an electrical current) generates a magnetic field and emits electromagnetic radiation. On the other hand, an electromagnetic radiation accelerates charged particles. These phenomena, the dynamics of free charges and currents, can be well described by Maxwell's equations [42]. These equations are considered as the foundation of classical electromagnetic theory and light-matter interaction because these equations pronounced the classical behavior of charges in electric and/or magnetic fields, both in vacuum and in materials. In the material media, the static and dynamics of the electromagnetic field can be described by the following Maxwell's equations [42, 43].

$$\vec{\nabla}\cdot\vec{\mathrm{D}} = \rho, \tag{3.1.1}$$

$$\vec{\nabla}\cdot\vec{\mathrm{B}} = 0, \tag{3.1.2}$$

$$\vec{\nabla}\times\vec{\mathrm{E}} = -\frac{\partial\vec{\mathrm{B}}}{\partial t}, \tag{3.1.3}$$

$$\vec{\nabla}\times\vec{\mathrm{H}} = \frac{\partial\vec{\mathbf{D}}}{\partial t} + \vec{J}. \tag{3.1.4}$$

Where $\vec{\mathrm{B}}$, $\vec{\mathrm{D}}$, $\vec{\mathrm{E}}$ and $\vec{\mathrm{H}}$ are the magnetic induction, electric displacement, electric field strength and magnetic field strength, respectively.

In the material media

$$\vec{\mathrm{D}} = \epsilon_0\vec{\mathrm{E}} + \vec{\mathrm{p}}, \tag{3.1.5}$$

$$\vec{\mathrm{B}} = \mu_0\vec{\mathrm{H}} + \mu_0\vec{\mathrm{M}}. \tag{3.1.6}$$

Here $\vec{P}$ and $\vec{M}$ are the electric dipole moment per unit volume (polarization) and magnetic dipole moment per unit volume (magnetization), respectively whereas ϵ_0 and μ_0 are permittivity and permeability in vacuum respectively [44, 45]. For non-conducting and non-magnetic media, the values of the electric charge per unit volume and the magnetization are zero. Therefore, the Maxwell's equations can be rewritten as follow [46]

$$\vec{\nabla}\cdot\vec{\mathrm{E}} = 0, \tag{3.1.7}$$

$$\vec{\nabla}\cdot\vec{\mathrm{H}} = 0, \tag{3.1.8}$$

$$\vec{\nabla}\times\vec{\mathrm{E}} = -\mu_0\frac{\partial\vec{\mathrm{H}}}{\partial t}, \tag{3.1.9}$$

$$\vec{\nabla}\times\vec{\mathrm{H}} = \epsilon_0\frac{\partial\vec{\mathrm{E}}}{\partial t} + \frac{\partial\vec{\mathrm{P}}}{\partial t}. \tag{3.1.10}$$

curl of Eq. (3.1.9) gives

$$\vec{\nabla}\times(\vec{\nabla}\times\vec{\mathrm{E}}) = -\mu_0\left(\vec{\nabla}\times\frac{\partial\vec{\mathrm{H}}}{\partial t}\right). \tag{3.1.11}$$

By applying curl properties and substituting Eq. (3.2.11) into Eq. (3.2.10), we can find the general wave equation of the electromagnetic field [45].

$$\vec{\nabla}^2\vec{\mathrm{E}} - \vec{\nabla}(\vec{\nabla}\cdot\vec{\mathrm{E}}) - \frac{1}{c^2}\frac{\partial^2}{\partial t^2}\vec{\mathrm{E}} = \frac{1}{\epsilon_0 c^2}\frac{\partial^2}{\partial t^2}\vec{\mathrm{P}}. \tag{3.1.12}$$

Where $\epsilon_0\mu_0 = \frac{1}{c^2}$, c is the speed of light in vacuum. Eq. (3.1.12) reveals that the propagation of the electromagnetic field depends on the electric dipole moment of the medium. The presence of polarization of the medium enables to explain optical effects such as dispersion and absorption. For electromagnetic field in which the charge density is zero, on account of Eq. (3.1.7), the general wave equation becomes

$$\vec{\nabla}^2\vec{\mathrm{E}} - \frac{1}{c^2}\frac{\partial^2}{\partial t^2}\vec{\mathrm{E}} = \frac{1}{\epsilon_0 c^2}\frac{\partial^2}{\partial t^2}\vec{\mathrm{P}}. \tag{3.1.13}$$

When the propagation of the radiation is taken place in vacuum, the wave equation becomes

$$\vec{\nabla}^2\vec{\mathrm{E}} - \frac{1}{c^2}\frac{\partial^2}{\partial t^2}\vec{\mathrm{E}} = 0. \tag{3.1.14}$$

For a wave propagating in the z-direction, the one-dimensional solution in free space is given by

$$\vec{\mathrm{E}}(z,t) = \varepsilon\vec{\mathrm{E}}_0\cos(\omega t - \kappa z). \tag{3.1.15}$$

Where ω and κ are the angular frequency and wave vector, and the phase velocity and wave vector are defined by

$$\mathrm{V}_p = \frac{\omega}{\kappa} \tag{3.1.16}$$

$$\kappa^2 = \frac{\omega_0^2}{c^2} \tag{3.1.17}$$

3.1.1 Schrodinger Equation

The electromagnetic radiation and matter interaction are manifested with absorption and emission processes. The absorption and emission of radiation due atomic transition is well explained by the time dependent Schrodinger equation. This fundamental equation is used to discuss the molecular transition from one state to another. When an atom which is initially at stationary state, $|k\rangle$ having energy E_κ is exposed to the electromagnetic radiation, it will be disturbed by an oscillating electric field of the electromagnetic radiation. Consequently, the molecule is subjected to jump to the other stationary state $|m\rangle$ and it will have energy E_m at the new stationary state [46, 47]. Before the molecular system is exposed to the radiation, the system can be described by

$$\hat{\mathrm{H}}^{(0)}\psi_k^{(0)}(x) = \mathbf{E}_k^{(0)}\psi_k^{(0)}(x). \tag{3.1.18}$$

Where $E_k^{(0)}$, $\psi_k^{(0)}(0)$ and $H_k^{(0)}$ are the energy eigen value, the wave function and the Hamiltonian of unperturbed molecular system at the stationary state $|k\rangle$. When the system is exposed to the electromagnetic radiation for a limited time, the electrons will jump to the other state, $|m\rangle$ and the system will be perturbed. This situation can be described by time dependent Schrodinger equation as follow

$$(\hat{H}^{(0)} + \hat{H})\psi(x,t) = i\hbar\frac{\partial}{\partial t}\psi(x,t). \tag{3.1.19}$$

Where $\hat{H}$ is the Hamiltonian that describes the interaction of the system and the radiation and $\psi(x,t)$ is the combination of the two stationary states. It can be described as

$$\psi(x,t) = P_k(t)\psi_k^{(0)}\exp^{[-iE_k^{(0)}t/\hbar]} + P_m(t)\psi_m^{(0)}\exp^{[-iE_m^{(0)}t/\hbar]}. \tag{3.1.20}$$

Where the coefficients $P_k(t)$ and $P_m(t)$ are the probability amplitudes of the two stationary states $|k\rangle$ and $|m\rangle$. If we consider that the transition is taken place between the two states only that is the decay to the other atomic level is neglected, the probability of finding the electron on either of the two states at a time t is 1 [46].

$$|P_k(t)|^2 + |P_m(t)|^2 = 1 \tag{3.1.21}$$

Where $|P_k(t)|^2$ and $|P_m(t)|^2$ represent the probability of finding an electron on the stationary states $|k\rangle$ and $|m\rangle$, respectively. Substituting Eq. (3.1.20) into Eq. (3.1.19) gives

$$(\hat{H}^{(0)}+\hat{H})\left(P_k(t)\psi_k^{(0)}e^{-i\mathbf{E}_k^{(0)}t/\hbar} + P_m(t)\psi_m^{(0)}e^{-iE_m^{(0)}t/\hbar}\right) = i\hbar\frac{\partial}{\partial t}\left(P_k(t)\psi_k^{(0)}e^{-iE_k^{(0)}t/\hbar} + P_m(t)\psi_m^{(0)}e^{-iE_m^{(0)}t/\hbar}\right) \tag{3.1.22}$$

Multiplying Eq. (3.1.22) with $\psi(x,t)$ conjugate and integrating in overall space followed by some mathematical activities results

$$i\hbar\frac{d}{dt}P_k(t) = P_k(t)\int \psi_k^*\hat{\mathrm{H}}\psi_k d\tau + P_m(t)e^{-i\omega_0 t}/\hbar \int \psi_k^*\hat{\mathrm{H}}\psi_m d\tau, \tag{3.1.23}$$

$$i\hbar\frac{d}{dt}P_m(t) = P_m(t)\int \psi_m^*\hat{\mathrm{H}}\psi_m d\tau + P_m(t)e^{-i\omega_0 t}/\hbar \int \psi_m^*\hat{\mathrm{H}}\psi_k d\tau. \tag{3.1.24}$$

Where

$$\omega_0 = \frac{E_m^0 - E_\kappa^0}{\hbar} \tag{3.1.25}$$

Eqs. (3.1.23) and (3.1.24) show the influence of the perturbation effect on the rate of transition from one system to another system [46]. These equations can be rewritten as

$$i\hbar\frac{d}{dt}P_k(t) = P_k(t)\mathrm{H}_{k\kappa} + P_m(t)e^{-i\omega_0 t}/\hbar\mathrm{H}_{km}, \tag{3.1.26}$$

$$i\hbar\frac{d}{dt}P_m(t) = P_m(t)\mathrm{H}_{mm} + P_m(t)e^{-i\omega_0 t}/\hbar\mathrm{H}_{mk}. \tag{3.1.27}$$

Where the matrix elements

$$\mathrm{H}_{kk} = \int \psi_k^*\hat{\mathrm{H}}\psi_k d\tau. \tag{3.1.28}$$

On the other side,

$$\vec{\mu}_{\kappa m} = -\vec{\mu}_{m\kappa} = -e\vec{\mathrm{E}}\int \psi_\kappa^*\hat{\mathrm{r}}\psi_m d\tau. \tag{3.1.29}$$

Eq. (3.1.29) describes the atomic transition dipole moment from stationary state $|k\rangle$ to another stationary state $|m\rangle$. It depends on the state wave functions $\psi_k(t)$ and $\psi_m(t)$ and the charge distributions in the states. The solutions of $p_k(t)$ and $P_m(t)$ shows the time evolution of the state wave functions. To proceed further with the atomic transition dipole moment, it is better to see the specific perturbation condition. For instance, if we consider a single mode radiation source, the x-component of the

radiation, that used as a source

$$\vec{\mathrm{E}}_x = \vec{\mathrm{E}}_0 \left(\frac{e^{i\omega t} - e^{-i\omega t}}{2} \right). \tag{3.1.30}$$

Then the Hamiltonian that governs this situation can be given by

$$\mathrm{H} = -\vec{\mathrm{E}}_x \cdot \vec{\mu}_x = -\vec{\mathrm{E}}_0 \left(\frac{e^{i\omega t} - e^{-i\omega t}}{2} \right) \cdot \vec{\mu_x}. \tag{3.1.31}$$

In order to substitute Eq. (3.1.31) into Eqs. (3.1.26) and (3.1.27), it is better to suppose at time t the atoms are at the lower state $|k\rangle$ and therefore, $P_k(0) = 1$ and $P_m(0) = 0$. We assume that the field amplitude is inadequately small and then for times $t < T$ [46]. So that the population of atoms at state $|k\rangle$ is still more whereas the population of atoms at a state $|m\rangle$ small. Based on this assumption Eqs. (3.1.26) and (3.1.27) become [48],

$$i\hbar \frac{d}{dt} P_k(t) = 0, \tag{3.1.32}$$

$$i\hbar \frac{d}{dt} P_m(t) = \frac{i}{2\hbar} \vec{\mathrm{E}}_0 \psi_m^{(0)} \left| \vec{\mu}_x \right| \psi_k^{(0)} \left(e^{it(\omega - \omega_0)} \right). \tag{3.1.33}$$

where

$$\int \psi_m^{(0)} \left| \vec{\mu}_x \right| \psi_k^{(0)} d\tau = \vec{\mu}_{km}. \tag{3.1.34}$$

Applying the initial condition, the integration over the time interval 0 and t results

$$P_k(t) = 0. \tag{3.1.35}$$

and

$$P_m(t) = \frac{\vec{\mathrm{E}}_0}{2\hbar} \vec{\mu}_{km} \left(\frac{e^{it(\omega_0 + \omega)} - 1}{\omega_0 + \omega} + \frac{e^{it(\omega_0 - \omega)} - 1}{\omega_0 - \omega} \right). \tag{3.1.36}$$

When the transition from $|k\rangle$ to $|m\rangle$ is taken place the atomic system absorbs energy from the electromagnetic field. Conspicuous absorption occurs if the field frequency ω approaches to transition resonance frequency ω_0. In the optical frequency range,

this indicates that $|\omega_0 - \omega| << \omega_0$. Therefore, the first term in Eq. (3.1.36) is then small compared to the first one and can be neglected.

Then

$$P_m(t) = \frac{\vec{\mathrm{E}}_0}{2\hbar}\vec{\mu}_{km}\left(\frac{e^{it(\omega_0-\omega)}-1}{\omega_0-\omega}\right) \tag{3.1.37}$$

Thus, the transition probability of the absorption from $|k\rangle$ to $|m\rangle$ state becomes

$$P_m^*(t)P_m(t) = \frac{\vec{\mathrm{E}}_0^2}{\hbar^2}\left|\vec{\mu}_{km}\right|^2\left(\frac{\sin^2\dfrac{(\omega_0-\omega)t}{2}}{(\omega_0-\omega)^2}\right) \tag{3.1.38}$$

If the deriving radiation is considered as electromagnetic waves of many frequencies, the probability of the transition becomes the sum of infinitesimal probabilities over the various frequencies. In this case, it is better to replace the energy density of electromagnetic wave ($u = \vec{\mathrm{E}}_0^2\varepsilon_0/2$) in the range ω andω and to integrate over the frequency spectrum. Since $u \to d\omega\rho(\omega)$ is slowly varying about and $\omega \approx \omega_0$. We can take out $\rho(\omega)$ outside of the integral.

$$P_m^*(t)P_m(t) = \frac{2\rho(\omega)}{\epsilon_0\hbar^2}\left|\vec{\mu}_{km}\right|^2\int\frac{\sin^2\dfrac{(\omega_0-\omega)t}{2}}{(\omega_0-\omega)^2}d\omega \tag{3.1.39}$$

$$\int\frac{\sin^2(ax)}{x^2}dx = 2\pi. \tag{3.1.40}$$

the probability finding the atom at state $|m\rangle$ in the time interval 0 and t becomes

$$P_m^*(t)P_m(t) = \frac{\pi\rho(\omega)}{\epsilon_0\hbar^2}\left|\vec{\mu}_{km}\right|^2 t. \tag{3.1.41}$$

Eq. (3.1.41) indicates that the probability finding an atom at the state$|m\rangle$ is lineally dependent to the time interval. For broad band excitation, rate of finding the atom at the stationary state $|m\rangle$ (rate of transition from state) $|k\rangle$ to $|m\rangle$ will be given by

$$\frac{d}{dt}(P_m^*(t)P_m(t)) = \frac{\pi\rho(\omega)}{\epsilon_0\hbar^2}\left|\vec{\mu}_{km}\right|^2. \tag{3.1.42}$$

Eq. (3.1.42) implies that the rate of transition probability depends on the transition moment and the energy density of the electromagnetic radiation. All the procedures presented have been taken place by considering the possibility of spontaneous emission from the upper state m to the lower energy state k, is negligible because we assumed that the population of atoms at the upper state is in significant. In case, there is a significant population of atoms at the beginning, the population of the upper state will be changed as a result of the induced absorption. The rate of change of population of the upper state is proportional to the radiation density $\rho(\nu)$ and the population of the lower state N_k. This can be described mathematical by

$$\left(\frac{dN_{km}}{dt}\right)_{absorbance} = N_{k\to m} = B_{km}\rho(\nu). \tag{3.1.43}$$

Where B_{km} is the Einstein coefficient. The population change in the upper state which is caused by the induced emission is given by

$$\left(\frac{dN_{km}}{dt}\right)_{emissin} = N_{k\leftarrow m} = -tA_{km}\rho(\nu). \tag{3.1.44}$$

Where A_{km} is the Einstein coefficient for spontaneous emission (Einstein A coefficient). In an equilibrium system, absorption and emission rates are equal and the net change of the population of the upper state is zero: this concept can be described by

$$\left(\frac{dN_{km}}{dt}\right) = 0. \tag{3.1.45}$$

On account of Eqs. (3.1.43) and (3.1.44), we can have,

$$N_{k\to m} + N_{k\leftarrow m} = 0 \tag{3.1.46}$$

and

$$(N_k - N_m)B_{km}\rho(\nu) = 0. \tag{3.1.47}$$

On account Eq. (3.1.43), when a molecular system is exposed to the electromagnetic radiation, there will be reasonable induced and spontaneous emissions that decrease the intensity of the absorption [48]. Since the only induced emissions travel parallel to the incident radiation and have the same phase, the net absorption intensity becomes the difference between the absorbed and induced emission intensities. It is described by

$$N_K B_{km}\rho(\nu) - N_m B_{mk}\rho(\nu) = B_{km}\rho(\nu)(N_k - N_m) \tag{3.1.48}$$

Eq. (3.1.48) describes that the intensity of absorption depends on the population difference of the lower and upper states. According to Plancks quantum theory, the radiation density emitted by the oscillators is given by [49]

$$\rho(\nu) = 8\pi h\frac{\nu^3}{c^3}\left[exp(h\nu/K_B T) - 1\right]^{-1}. \tag{3.1.49}$$

and Einstein A_{km} coefficient is related with Einstein B_{km} coefficient as

$$A_{km} = \frac{8\pi h\nu^3}{c^3}B_{km}. \tag{3.1.50}$$

On the other hand, Einstein A_{km} coefficients can be related to the integrated absorption coefficient as

$$A_{mk} = \frac{8\pi c\ln 10}{N_A}\frac{\nu^2}{c^2}\int \varepsilon(\nu)d\nu. \tag{3.1.51}$$

3.1.2 Beer-Lambert's Law and Integrated Absorption Technique

In absorption spectroscopy, the Beer-Lambert's law is used to associate the absorption of light to various properties of the matter through which the light travels. Based on Beer's law, the absorbance, A, is related to the incident light intensity, I_0 and

transmitted light intensity (I) by

$$A = \log \frac{I_0}{I}. \tag{3.1.52}$$

Here the ration of the transmitted light intensity and incident light intensity is referred as transmittance, T of the sample [1, 49]. That is

$$T = \frac{I}{I_0}. \tag{3.1.53}$$

Beer's law also relates the absorbance with path length, l, molar extinction coefficient, ε, and absorption coefficient, α, as follows

$$A = \varepsilon l C. \tag{3.1.54}$$

$$A = \alpha l. \tag{3.1.55}$$

Where C is the concentration of the sample. Furthermore, Beer's law associates the ration of the incident intensity and the transmitted intensity with absorption cross section, σ, and the number molecules per unit volume, N, as

$$\frac{I}{I_0} = e^{-\sigma N l}. \tag{3.1.56}$$

Eqs. (3.1.54), (3.1.55) and (3.1.56), indicate that once we take absorbance measurement, we can determine the molar extinction coefficient, ϵ, absorption coefficient, α, and absorption cross section, σ. The absorption coefficient, α, at a single frequency can be expressed in terms of absorption cross section, σ, and the number molecules per unit volume, N, by

$$\alpha(\nu) = \sigma(\nu) N. \tag{3.1.57}$$

When the incident light is released to the sample of the molecule, the absorption may be taken place within certain frequency range rather than at a single frequency.

Therefore, the absorption coefficient calculated for single frequency by Eq. (3.1.57) may not well express absorption intensity of molecular transition. So that we have to use the integration absorption techniques in order to calculate the absorption coefficient which is due to all frequencies in the band [50]. This technique is independent from the line function shape that can be varied due the change in pressure, concentration, temperature and solute solvent interactions. According to the integrated absorption technique, the integrated absorption coefficient, $\alpha(t)$ can be calculated by

$$\alpha_t(\nu) = \int \sigma(\nu) d\nu. \tag{3.1.58}$$

On account of Eqs. (3.1.52), (3.1.54), (3.1.55), Eq. (3.1.58) will be

$$\alpha_t(\nu) = \frac{1}{l} \int \log\left(\frac{I_0}{I}\right) d\nu. \tag{3.1.59}$$

Moreover, the integrated absorption technique is used to obtain the integrated absorption crosssection, $\sigma(t)$, as

$$\sigma_t(\nu) = \frac{1}{Nl} \int \log\left(\frac{I_0}{I}\right) d\nu. \tag{3.1.60}$$

3.1.3 Oscillatory Strength

Oscillator strength refers the average number excited electrons per atom of the molecule. This parameter is used to indicate the strength of the probability of the electrons transition and it can be determined directly from absorption measurement. It can be related with the molar decadic absorption coefficient by

$$f = 4.32 \times 10^{-9} \frac{molcm}{L} \int \varepsilon(\nu) d\nu. \tag{3.1.61}$$

Moreover, the oscillatory strength can be expressed in terms of the absorption coefficient and number density as [42].

$$\int \varepsilon(\nu)d\nu = 2.65 \times 10^{-6} Nf. \tag{3.1.62}$$

3.1.4 Matrix Elements of the Transition Dipole Moment

The transition dipole moment $\vec{\mu}_{km}$ is a vector that describes the strength of the interaction of light with matter. It is described as [6]

$$\vec{\mu}_{km} = \int \psi_k^* \vec{\mu} \psi_m d\tau \tag{3.1.63}$$

The transition dipole moment is used to obtain the selection rules that is if $\vec{\mu}_{km} = 0$, there is no transition between the initial and final states. This implies that there is no light-matter interaction which is strong enough that cause electrons to escape from one stationary state to another and if $\vec{\mu}_{km}$ is large, the atomic transition probability becomes large.

3.2 Fluorescence Quenching Mechanisms

When a molecule absorbs light, an electron is exited to a higher state. The excited electron then relaxed to the lower sate and the excited state become depopulated. The depopulation of the excited states can be taken place in several ways [51]. For instance, it may be internal conversion, intersystem crossing, phosphorescence or fluorescence. The relaxation of electrons from the lowest vibration level of the excited state to the ground state by giving up their excess energy as photons is called fluorescence. The fluorescence of the fluorophor is characterized by the parameters such

lifetime, intensity and quantum yield. The fluorescence lifetime τ_0 refers the duration for how long the fluorophore stays in the excited state [52]. The intensity of the fluorescence at a given wave length is given by

$$F_f = nE. \tag{3.2.1}$$

The fluorescence quantum yield is given by

$$\Phi_f = \frac{NMF}{TNEM}. \tag{3.2.2}$$

Where NMF and $TNEM$ represent the number of molecules that fluorescence and total number of excited molecules respectively.

Or, it can be expressed as

$$\Phi_f = \frac{photonsemitted}{photonsabsorbed}. \tag{3.2.3}$$

Where F_f, n, E and Φ_f are the fluorescence intensity, the number of emitted photons, the photon energy and quantum yield, respectively. When the external molecules are added to the fluorescence system, the fluorescence intensity and the fluorescence quantum yield of the fluorophores decrease. This is referred as fluorescence quenching whereas the external molecules that render the intensity of the fluorophere and the quantum yield to be decreased is known as quenchers [53]. The chemical properties of the molecules and nearby environment of the fluorophore determine the mechanisms of quenching. Since fluorescence is a sensitive technique, various factors can affect the quenching mechanisms. Due to this taking the detail analysis about the mechanisms of quenching is very complex [54].

Generally, the quenchers will decrease the intensity of the fluorescence by either making collision with the fluorophores or by forming the nonfluorescent complex

with the fluorophores. According to the way that the quencher interacts with the fluorophore, the quenching mechanism will be dynamic or static [55]. If the intensity is decreased due to the collision that exit between the quencher and fluorophore it, we say that the dynamic quenching and if it is due to the formation of the ground complex it is static quenching. In order to demonstrate the impact of the quencher on the three fluorescence parameters that is intensity, lifetime, and quantum yield, it is better to consider that there are m number of fluorophore molecules [56]. At a specific emission wavelength, the measured intensity is proportional to the number of emitted photons. But in dynamic or static quenching, a number of photons emitted become fewer, and then the quantum yield will be decreased. Since the intensity and quantum yield are direct proportional, a decrease in quantum yield will be accompanied by a decrease in intensity of fluorescence. For given solution that contains m number of fluorophore molecules, the fluorescence lifetime for each molecule is the same. When static quenching occurs, some of the fluorophore molecules bind to the quencher and form nonfluorescent complex with the quencher do not fluoresce. Therefore, in static quenching, the number of molecules that are still fluorescing is less than m number of molecules. However, all them have the same fluorescence lifetime. As a result, the calculated mean life time of fluorophore in the static quenching will be equal to the measured life time in the absence of the quencher. Consequently, the quantum yield and fluorescence intensity decrease in static quenching whereas the fluorescence lifetime does not change. The direct physical interaction between the fluorophore and the quencher is not obligatory for the presence of static quenching rather we can see a long- or short-distance effect, depending on whether the fluorophore is within the interaction area or not [57].

In the case dynamic quenching the complex formation is not induced instead the fluorophore and quencher are collided. Owing to this, there will be a loss of fluorophore energy, the decreasing of the fluorescence intensity and then the two molecules are again separated. Thus, dynamic quenching is accompanied with a partial energy loss of the fluorophore molecules while entering into collision with the quencher molecules. This indicates that the molecules which are not participating in the collision process have less fluorescence life time than free molecules in solution. As a result, the mean fluorescence lifetime measured in the presence of collision quenching becomes less than the mean lifetime measured in the absence of the quencher [58]. Also, all the fluorescence parameters are affected by a thermal quenching. The life time intensity and quantum yield are decreased with increasing temperature. In fact, the decrement is governed by the dynamics of the surrounding environment of the fluorophore.

3.2.1 Collisional Quenching

Macromolecules exhibit two types of continuous motions that the molecule can rotate on itself, following the precise axis of rotation, and it can have a local flexibility [59]. Local flexibility refers the internal motions small molecules. For instance, solvent molecules can diffuse into the macromolecules. In general, this diffusion enables the solvent molecules to reach into the interior hydrophobic core of macromolecules [60]. This denotes that the term hydrophobicity is a relative and not absolute. The internal dynamics of macromolecules permit and facilitate a permanent contact between the core of the macromolecules and the solvent and allow the small molecules such as oxygen to diffuse within the core of the macromolecules [61]. Dynamic quenching

occurs during the exited state life time. In the collisional quenching process, the excited state become depopulated parallel to the other processes such as intersystem crossing, internal conversion, etc. Consequently, the fluorescence life time of the excited state becomes less in the presence of a collisional quencher than the absence of it [62]. The velocity of fluorophore de-excitation can be given by

$$V = K_q[F][Q]. \tag{3.2.4}$$

Where K_q is the bio-molecular quenching constant, $[F]$ is the fluorophore concentration and $[Q]$ is the concentration of the quencher. The quantum yield in the absence of quencher is given by

$$\Phi_F = \frac{K_r}{K_r + K_i + K_{isc}}. \tag{3.2.5}$$

where K_r, K_{isc} and K_i are the radiative constant, the inter-system crossing constant and the constant corresponding to de-excitation due to the temperature effect. In the presence of quencher, the quantum yield becomes

$$\Phi_{F(Q)} = \frac{K_r}{K_r + K_i + K_{isc} + K_q}. \tag{3.2.6}$$

As it is clearly stated in [63], the ratio of Eqs. (3.2.5) and (3.2.6) gives

$$\frac{\Phi_F}{\Phi_{F(Q)}} = 1 + K_q\tau_0[Q] = 1 + K_{SV}[Q]. \tag{3.2.7}$$

On the other hand, the Stern-Volmer equation can be expressed by the ration of intensities as follow:

$$\frac{F_0}{F} = 1 + K_q\tau_0[Q] = 1 + K_{SV}[Q]. \tag{3.2.8}$$

Where F_0 and F are the intensity of fluorophore in the presence and absence of the quencher respectively and

$$\tau_0 = \frac{1}{K_r + K_i + K_{isc}}. \tag{3.2.9}$$

Here τ_0 is the mean fluorescence lifetime of the fluorophore in the absence of quencher and K_{SV} is the Stern-Volmer constant. K_{SV} can be determine from $\frac{F_0}{F}$ versus [Q] graph. The slope of this graph represents K_{SV}. The values of K_{SV} and K_q give gives an idea about the importance of fluorophore availability to the quencher and the importance of diffusion of the quencher within the medium respectively.

3.2.2 Static Quenching

It is the mechanisms of quenching which is due to the formation of the nonfluorescent complex on the ground state. When nonfluorescent complex absorbs light, it returns to the ground state without emitting any photons [62]. So this type of quenching is called static quenching. Mathemically it can be described as

$$C + Q \leftrightarrow CQ. \tag{3.2.10}$$

The associating constant K_a can be given by

$$K_a = \frac{[CQ]}{[C]_f[Q]_f}. \tag{3.2.11}$$

Where $[CQ]$ is the complex concentration, and $[C]_f$ and $[Q]_f$ are the concentrations of free fluorophore and quencher. Since the total fluorophore concentration is

$$[C]_0 = [C]_f] + [CQ]. \tag{3.2.12}$$

and bound fluorophore does not fluoresce, substituting Eq. (3.2.12) into Eq. (3.2.11) following by some mathematical steps yields

$$\frac{[C]_0}{[C]_f} = 1 + K_a[Q]_f \tag{3.2.13}$$

and

$$\frac{[F]_0}{[F]} = 1 + K_a[Q]_f. \tag{3.2.14}$$

If we consider the concentration of fluorophore bound to quencher to be very small in contrast to the concentration of the added quencher, the concentration of free quencher will be equal to the total added concentration. Thus, Eq. (3.2.14) can be written as

$$\frac{[F]_0}{[F]} = 1 + K_a[Q]. \tag{3.2.15}$$

Therefore, the association constant K_a will be determined from $\frac{[F]_0}{[F]}$ versus $[Q]$ because the slope of $\frac{[F]_0}{[F]}$ versus [Q] stands for K_a. In static quenching, we can see the fluorescence of free fluorophore in solution but the complexed fluorophore does not fluoresce and thus we cannot observe in the derived equations. Therefore, the fluorescence lifetime of free fluorophore is the same whether all fluorophore molecules are free or some are complexed. Thus, the fluorescence lifetime of fluorophore does not depend on the concentrations of quencher. This implies the following equation:

$$\frac{\tau_0}{\tau_{(Q)}} = 1. \tag{3.2.16}$$

Here $\tau_{(Q)}$ is the fluorescence lifetime the fluorophore when some of the fluorophores are complexed with the quencher. Therefore, in static quenching only the intensity is decreased but the intrinsic fluorescence lifetime is not changed [64]. Static quenching is a typical mechanism to investigate the interaction between two macromolecules, between macromolecules and nanoparticles, or between drugs and nanoparticles. The binding parameters of the fluorophore-nonfluorophore complex can be determined because of the fluorescence modification of the fluorophore observables. Finally, we should note that dynamic quenching is diffusion-dependent but not static quenching. Thus, increasing the temperature makes an increase the diffusion coefficient. However, in case of static quenching, increasing the temperature destabilizes the formed complex and thus decreases its association constant [65].

3.2.3 Fluorescence Resonance Energy Transfer (FRET)

The extensive use of fluorescence resonance energy transfer (FRET) is owing to the encouraging distances, which is approximated to the size of protein for energy transfer. In addition, the degree of FRET is favorably expected from the spectral properties of the fluorophores. It means that if the spectral properties of the fluorophores permit FRET, it will happen in the samples of the biomolecule moreover it will not be considerably influenced by the biomolecules [66]. These encouraging properties are used to design experiments based on the known sizes and structural features of the sample. Since FRET is s an electrodynamic phenomenon, it can be explained by the principles of classical physics. In FRET, the absorption spectrum of the acceptor overlaps with the emission spectrum. The rate of energy transfer depends on extent of overlapping between emission spectrum of the donor and the absorption spectrum of the acceptor, the quantum yield of the donor, and the distance between the donor and acceptor [66]. The distance dependence of the rate of energy transfer enables us to measure the distance between donors and acceptors and thus the main application of rate of energy transfer is to measure the distance that exists between the sites of a macromolecule particularly in the study of protein structure [67]. In protein structure study, the donor is always a tryptophan residue but sometimes extrinsic donors are also used because these have better opportunities to position the donor in preferring the location to select the DA pairs that are most appropriate for a particular application. From the energy transfer efficiency, DA distance can be determined if the DA is not changed during the excited state lifetime and if there are a single donor and single acceptor [68]. On the other hand, the energy transfer efficiency can be determined, using the steady-state measurements of the extent of quenching the donor by

acceptor even the actual DA distance is not being measured. DNA hybridization or any bioaffinity reactions are typical experiments in which energy transfer efficiency is determined without any steady-state measurement [69]. If the sample consists of two types of macromolecules that are separately labeled as donor and acceptor, an association of the macromolecules can usually be observed using RET. The observation of RET is adequate to measure the degree of binding, even without calculating the DA distance. Moreover, resonance energy transfer is also used to investigate the binding which occurs between macromolecules, between macromolecule and nanoparticles and nanoparticles and drugs when there is more than a single acceptor near a donor [70].

Chapter 4

Materials and Methods

4.1 Materials

4.1.1 Chemicals

Zinc acetate (99% pure) and sodium hydroxide (99% pure) were bought from Merck, Germany, Ferulic acid (98% pure), dibasic sodium phosphate (99.95% pure) and monobasic sodium phosphate (99% pure) were purchased from Sigma-Aldrich. We used distilled water as a solvent.

4.1.2 Apparatus and Instruments

Some of the basic apparatus and instruments used during the experiment are measuring pipettes, volumetric flasks, magnetic stirrer with hot plate, digital balance with accuracy of 0.0001 g, beakers, 5 mm size of quartz glass cuvettes, pestle mortar, stand, burette spatula, tongs and Elmmasonic P300H sonicator. For electronic absorption and fluorescence measurements, we used Ocean Optics Spectrophotometers

(JAZ 3-chanel) and Varian Cary Eclipse Fluorescence Spectrophotometer, respectively, Circular Dichroism Spectrophotometer (CD) J-1500, Jasco which is equipped with thermostat was used for the electronic absorption measurement solution of ferulic acid.

4.2 Experimental Procedures

Under this section experimental activities are outlined. This includes zinc oxide nanoparticles synthesis approach and binding measurement approach.

4.2.1 Synthesis of Zinc Oxide Nanoparticles

ZnO NPs used in the present study were prepared by sol-gel method. 12 g of Zinc acetate dehydrate $Zn(CH_3COO)_2.2H_2O$ and 6 gm Sodium hydroxide NaOH were dissolved in de-ionized water. The solutions were stirred with a magnetic stirrer at 50 ^0C with 1000 rpm for 50 minutes and 25 minutes separately. Then sodium hydroxide solution is added to the solution of zinc acetate drop wisely for 20 minutes. The mixed solution was heated under the continuous string for an hour at 50 ^0C with 1000 rpm. The resulting white gel was filtered, and washed with de-ionized water 7 times. After washing, the gel was made to dry at 65 ^0C for 18 hours on hot plate in BP110 Laboratory Grade Microwave. finally we grinded it.

4.2.2 Binding Measurement

The stock solution of FA ($1.54 \times 10^{-5}M$) was prepared in sodium phosphate buffer solution with 6.8 PH and the solution of ZnO NP was prepared in de-ionized water.

Firstly, the absorbance and emission of the ferulic acid solutions were measured in the wavelength range of 220 to 400 nm and 250 and 450 nm by Ocean Optics Spectrophotometers (JAZ 3-chanel) and Circular Dichroism (CD) J-1500, Jasco Spectrophotometer, respectively.

After taking these measurements, different amount of ZnO NPs solution ranging $(2.5 - 17.5) \times 10^{-5} M)$ were added to a fixed amount of FA solution with concentration $(1.54 \times 10^{-5} M)$ and sonicated well.

The fluorescence measurements for the mixed solution were carried out by Circular Dichroism (CD) J-1500, Jasco Spectrophotometer and the spectra were recorded from 250 to 450 nm with an excitation wavelength of 280 nm which is the absorption maxima of ferulic acid at the concentration $(1.54 \times 10^{-5} M)$ at three different temperatures 298, 310 and 316 K.

4.2.3 Absorbance Measurment of Ferulic Acid

The stock solution of FA with concentration $3.01 \times 10^{-3} M$ was prepared and then the working solutions of FA with seven different solutions in the concentration range $(8.42 - 23.8) \times 10^{-5}$ M and 7.86×10^{-5} M solution were prepared from stock solution. The absorbance measurement of the samples in the concentration range $(8.42 - 23.8) \times 10^{-5}$ M and at a particular concentration 7.86×10^{-5} M have been carried out at room temperature in order to deal with the self-associations and optical transition properties of FA, respectively.

Furthermore, 9.02×10^{-5} M solution of FA was prepared in order to study the impact of the temperature variation on the dimerization constant, dimer extinction coefficient and monomer extinction coefficient and also the thermodynamic properties of FA. The

spectra were recorded with a spectral bandwidth of 3 nm and a scanning speed of 20 nm/min in the wavelength range 250 to 400 nm. The spectrum of pure solvent (water) was subtracted from that of the solution containing FA.

4.3 General Synthesis Approach and Spectroscopic Techniques

4.3.1 Methods of Synthesis

Generally, there two types of synthesis methods in nanomaterials fabrication, top-down and bottom-up. Top-down approach can be taken place by successively cutting bulk materials. In this case the physical process such as attrition, milling or crushing are widely utilized in synthesizing nanoparticles. It is used in solid state materials processing. It is not the preferable approach because it is difficult to fabricate uniformly shaped nanomaterials and it is not easy to realize small nanoparticles. For instance, imperfections of surface structure is the main limitation of this approach. These imperfections in turn lead to extra challenges in device designing and fabrication [71].

In bottom-up approach, nanoparticles fabrication can be taken place by atom by atom, molecule by molecule or cluster by cluster building. It is commonly used for synthesizing most of the nano-scale materials. Here, we can realize to generate a uniform size, shape and distribution of the nanomaterials. It effectively covers chemical synthesis. The choice of synthesis technique is one of the key factor to find the nanoparticles in such a way that we want [72].

4.3.2 Sol-gel Method

The sol-gel method is a chemical technique used for synthesizing various oxide materials [73]. In this case, precursors consist of a metal or metalloid element surrounded by various reactive ligands. In a typical sol-gel process, hydrolysis and polymerization reactions of the precursors are carried out. The hydrolysis reaction and polymerization reactions result a colloidal suspension, or a sol and inorganic metal salts or metal oxides. Then after, the sol gradually evolves toward the formation of a gel containing both liquid and solid phases. the morphologies of the sol will be in the range from discrete particles to continuous polymer networks. The sol-gel transition controls the particle size and shape and calcination of the gel produces the oxide [74]. This method has more advantages than other methods, because it allows impregnation or co-precipitation, which can be used to introduce dopants. Moreover, using this method, we can overhand the texture, morphological and chemical properties the nonmetallic inorganic materials such as ceramic materials at low temperatures is possible compared to the high temperature processes [75]. The sol-gel parameters such as types of solvent, concentration of the precursors acid or base content, water content, the concentration of precursor and temperature are the main factors that play great role in determining the properties of the gel. Moreover, sol-gel parameters affect the structure of the initial gel and the properties of the synthesized material at all subsequent processing steps. After gelation, the wet gel can be optionally aged in its mother liquid, or in another solvent, and washed [76]. The time spent for the formation of a gel and its drying is referred as aging. Aging is also another sol-gel parameter [77]. Sol-gel method is more preferable by many chemists because it is environmentally friendship, less toxic. As a result, it is widely applied to prepare oxide

materials. Moreover, using this method, synthesis of nonmetallic inorganic materials such as ceramic materials at low temperatures is possible compared to the high temperature processes. In this work, we used sol-gel approach to synthesize zinc oxide nanoparticles using zinc acetate and sodium hydroxide as precursors.

4.3.3 Basic Components and Experimental Set Up of Microscopic and Spectroscopic Instruments

Nanoparticles characterization concerns properly on the crystal structure and on chemical composition of nanoparticles as the first step after nanoparticle synthesis. In addition, it emphasizes the study of parameters such as size, shape size distribution, degrees of agglomeration, the surface chemistry, absorbance and the emission properties. These properties may affect the other properties of the nanoparticles. Moreover, these properties also determine the application of nanoparticles. Until now, there were no standardized protocols for this aim. Credible and vigorous measurement methods for NPs will seriously affect the using up of the nanoparticles in commercial applications and consent to the industry comply with the regulation. The deficiency of appropriate reference materials for the standardized analytical tools, the interdisciplinary nature of the field, the difficulty of sample preparation are the basic challenges in the analysis of nanomaterials and the interpretation of the data. The measurement of the concentration of the nanoparticles in situ and machine accessible particularly in scaling up production is still an unaddressed challenge in nanoparticle characterization. Besides, the wastage and sewage from mass production must be monitored. In order to scale up the manufacturing of nanoparticles, the quantification techniques must be required. While we characterize nanoparticles, we should

give attention to the surface of the ligands that influence the physical properties of the nanoparticles. In this thesis, various spectroscopic and microscopic techniques are used to characterize the structural and optical properties of zinc oxide nanoparticles, to probe the optical properties of ferulic acid, to investigate the binding of the ferulic acid with zinc oxide nanoparticles. The details of the techniques are outlined below

4.3.4 XRD Analysis

X-ray diffraction (XRD) technique is used widely for characterizing nanoparticles. XRD measurement provides the information about the nanoparticles particularly the crystalline nature, nature of phase, lattice parameters, the composition and the crystalline grain size. When an x-ray beam is injected into the nanomaterial sample, it would be scattered by the sample. If two or more x-ray beams scattered by the samples that have some phase differences are superimposed onto each other, diffraction has occurred. The x-ray diffraction instrument is used to collect the intensities of the scattered signals. When the intensities of the scattered signal are collected by x-ray diffraction, we can get the diffraction pattern of the measured sample. The pattern will be intensity versus the phase angle [78]. By applying this pattern in the crystal surface regulation process for the sample, the materials crystalline structure, such as the orientation and phase angles, can be obtained. By comparing the position and intensity of the peaks of the measured sample with the reference patterns available from the International Centre for Diffraction Data (ICDD, formerly branded as Joint Committee on Powder Diffraction Standards, JCPDS) database, the composition of the particles can be determined [79]. Based on JCPDS the phase will also be identified. An advantage of using x-ray diffraction measurement is that it can analyze the

material without causing damages on the material [40]. In this thesis, we used an x-ray diffraction machine, called the Rigaku SmartLab which is equipped with xpert software.

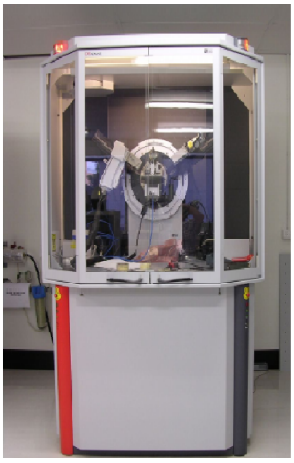

Figure 4.1: Rigaku SmartLab X-ray diffraction machine.

4.3.5 Scanning Electron Microscopy (SEM)

Scanning electron microscopy (SEM), is a powerful surface imaging method that generates a signal which gives clear information for the atomic composition and the morphological details about the surface of the specimen [80]. Scanning electron microscope uses the electrostatic lenses and beams of accelerated electrons that have much shorter wavelength than visible light photons to produce images with higher resolution, higher magnification and deep focus. Scanning electron microscope is more preferable to the optical microscopes because its resolution can be extended to a few nanometers and its magnifications can be adjusted from 10 to 300,000 times. The image resolution obtained by the scanning electron microscope depends on both the

property of the electron probe and the interaction of electron probe with the specimen. In SEM, electron beam which is accelerated by a relatively low voltage (1-20 kV), can be scanned on the specimen surface [81]. As the electron beam strikes the surface, a large number of signals are generated through the surface in the form of electrons or photons. The size distribution and shape of nanomaterials, the process of drying and contrasting samples conductivity and non-conductivity properties of the specimen are the main factors to have good image about the surface. The process of drying and contrasting shrink the specimen and the characteristics of the nanomaterials sample will be changed. The nonconductive samples have a tendency to attain charge and inadequately deflect the electron beams. As a result, we may have fault images. So, the samples should be coated by electrically conducting material. In this study, we used the scanning electron microscope to take the image of the morphology of zinc oxide nanoparticles [82].

4.3.6 FTIR Spectrophotometer

FTIR spectroscopy is the non-destructive characterization method, which is very versatile to surface characterization of nanoparticles [80]. It is used to study the vibrational changes of the motion of atoms in a molecule.

The motion of atoms in a molecule investigated by taking the measurement of the absorption of electromagnetic radiation with wavelengths near IR, mid IR and far IR. IR covers a spectral region from the red end of the visible spectrum (12500 cm^{-1}) to the microwave (10 cm^{-1}) regions in the electromagnetic spectrum. It is easily divided into near IR (12500 to 4000 cm^{-1}), mid IR (4000 to 400 cm^{-1}) and far IR (400 to 10 cm^{-1}). In vibrational spectroscopy, the recorded spectrum which is intensity

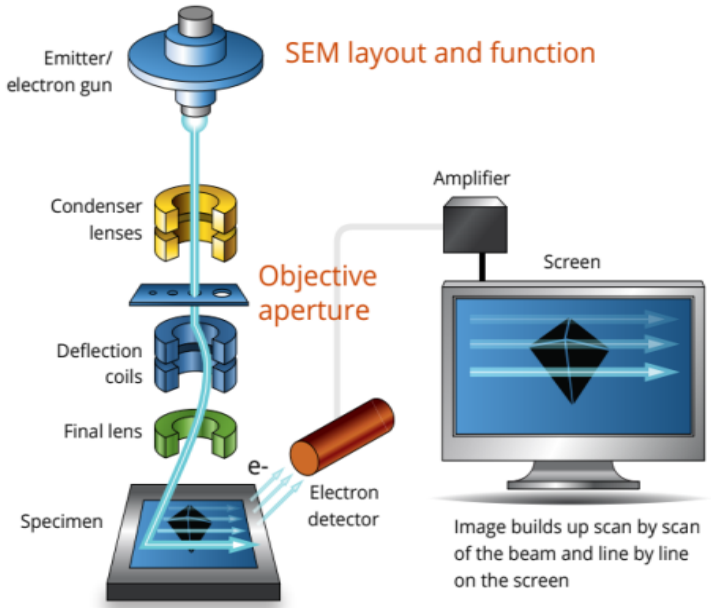

Figure 4.2: Schematic diagram of SEM.

versus the wave number provides the information about the motion of atoms in a molecule, the geometrical arrangement of atoms, the position of bands that is related to the strength and nature of bonds and specific functional groups providing thus information concerning molecular structures and interactions [54, 83]. If a molecule absorbs IR radiation, the vibration will modulate the vibrating molecule molecular dipole moment and the molecule becomes IR active.

Vibrational spectroscopy is used to study the vibrational changes of the motion of atoms in a molecule. In this case, we look at the changes in vibration motion of atoms in a molecule, which are greatly governed by the geometrical arrangement of atoms, their mass and the strength of the chemical bonds that exist among them. So that using this spectroscopy, we can determine the chemical composition of the nanoparticles surface, adsorbents on the surface, we can detect volatile reaction products and

we can also identify the surface reactive sites that play a role for the surface reactivity. On the other hand, the surface properties of the nanoparticles greatly monitor the overall properties of the material. As a result, FTIR spectroscopy has a direct application in the optimization of the gas sensors of nanoparticles.

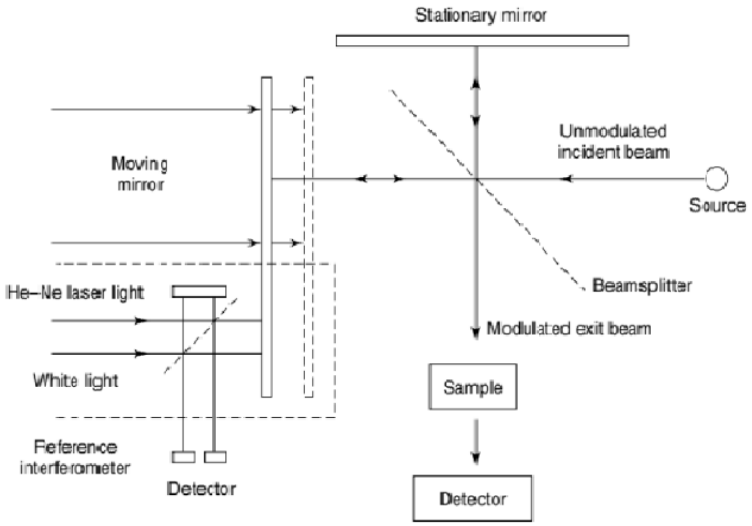

Figure 4.3: Schematic diagram of FTIR.

4.3.7 UV-Vis Spectroscopy

Many molecules absorb ultraviolet (UV) or visible light. When the molecule absorbs ultraviolet or visible radiation, outer electrons of the ground state will jump from the ground state to excited state.

As it is clearly depicted, in Eq. (3.1.54), the Beer-Lambert's law forms the mathematical physical basis for the light absorption measurements of the solution of the sample. That is according to Eq. (3.1.54), absorbance is directly related to the concentration of the sample c and the path length l. Absorption strongly depends on the

types of samples and the environment of the sample, the structural groups present within the molecules, the number of absorption bands in the absorption spectrum, the solvent by which the absorbing substance is dissolved and the size of the particle is also imperative. If the dimension of the particle $s >> \lambda$, and when light interacts with the samples instead of absorption some parts of the light will be scattered and reflected. When the samples are solids, light penetrates into the sample accompanied by numerous reflections, refractions and diffraction and emerges finally scatter at the surface.

In this thesis, we used ocean optics spectrometers and circular dichroism spectrophotometer to measure the absorbance of zinc oxide nanoparticle and the absorbance of ferulic acid, respectively.

4.3.8 Ocean Optics Spectrometers

It is a quick, an easy and a portable spectrophotometer that is used for generating spectra in the visible, UV and near-infrared (near-IR) regions of the electromagnetic spectrum. In this spectrometer (grating, mirrors, slit and detector) are accommodated in an optical bench which can be handled with our palm. The components of the ocean optics spectrophotometry includes spectrometer AC power supply cuvettes One USB cable and computer equipped with an ocean optics software

In typical absorbance set-up of ocean optics spectrophotometry, the light source sends light through an input fiber into a cuvette in a cuvette holder, the light interacts with the sample and then the output fiber carries light from the sample to the spectrometer which is connected to the computer [63].

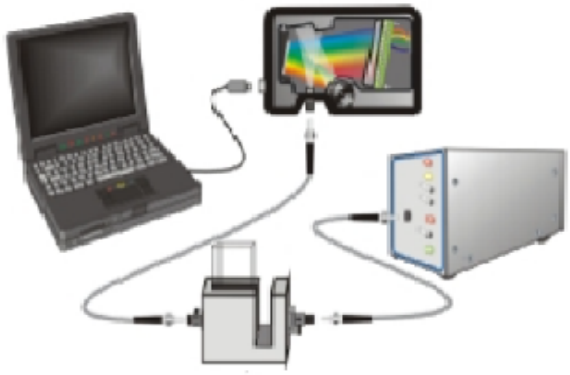

Figure 4.4: Ocean optitcs spectrophotometer set-up.

4.3.9 Circular Dichroism (CD)

CD is one of the typical instruments that is used to characterize the structure of molecules through different absorptions of circularly polarized lights in left-handed direction (LCPL) and in right-handed direction (RCPL) on the asymmetric molecule. Circular dichroism is used to measure the absorbance of the sample is called CD absorption spectrophotometer. It uses xenon lamp (which is polychromatic light) as source. This polychromatic light is converted to monochromatic and then further to linearly polarized light by the polarizer.

The linearly polarized light is brougth in to pass through the modulator. The modulator converts the polarized light into LCPL and RCPL alternatively. Both LCPL and RCPL pass through the sample and their absorbance is recorded. Since CD spectroscopy a quick, nondestructive tool it is more preferable technique to study conformational behavior of biomolecules, the structures of drug-delivery nanocarriers, the interactions of nanocarriers with biomolecules and donor-acceptor interactions such as protein-DNA, DNA- ligand, protein-protein and protein-ligand interactions

[84]. There are, however, several limitations to this technique. For instance, it is less sensitive than absorption spectroscopy by two to three orders of magnitude due to differential absorption of left and right circularly polarized radiation, there is a problem in analyzing CD spectra obtained in a complex of a chiral compartment adhering to a chiral receptor which usually appears in macromolecules and nanomaterials, it cannot show the actual contribution made by any particular amino-acid residue in a protein-type biomolecule to form a CD spectrum and CD measurement reveals weak spectra if the sample contains only non-chiral chronophers. But some of these limitations can be eliminated by applying different CD-based techniques, such as fluorescence detected CD that enhances sensitivity, and magnetic CD to detect molecules that lack a chiral center [85].

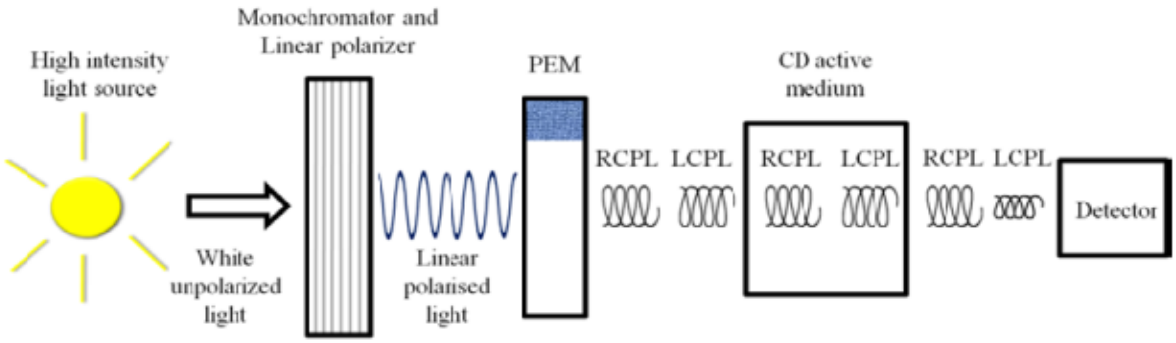

Figure 4.5: Schematic diagram of CD spectrophotometer.

4.3.10 Photoluminescence Spectroscopy

Photoluminescence (PL) is a powerful technique to study optical properties of semiconductors [86]. PL is involved with emission of radiation from the semiconductors.

When light with photon energy higher than the band gap of semiconductor is irradiated to the sample, electrons on the ground state will be excited to a higher energy state, and after losing some energy, the excited electrons turn back to the ground state. This process is accompanying with the emission of photons. PL is used to extract worthful data concerning to semiconductor sample composition, quantum well thickness or quantum dot sample monodispersity [87]. Particularly, from low-temperature PL spectra, we can get more detailed information about the semiconductors. The data extracted from an emission spectrum is used to compare electronic properties of the material. Time-resolved photoluminescence, is used to identify the radioactive decay of the samples. The spectrum which stands for the intensity of light which is diagrammed against the wavelength is vital to determine the electronic structure and properties of materials that affords the peak light intensity that materials are able to emit for a given wavelength. For instance, it is possible to observe material imperfections and impurities and in some case, it is used to estimate the band gap properties of the semiconductor.

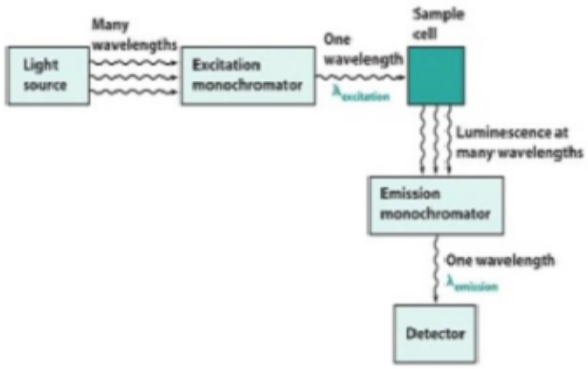

Figure 4.6: Schematic diagram of fluorescence spectrophotometer.

Chapter 5

Results and Discussion

5.1 Characterization of ZnO Nanoparticles

5.1.1 XRD Analysis

The structural characteristics of the prepared nanoparticles were carried out using x-ray diffractometer (Rigaku SmartLab) with Cu $K_{\alpha 1}$ radiation source ($\lambda = 0.1541\ nm$) and 3^0/min angle of rotation of goniometry speed in the 2θ range from 15^0 to 90^0. The XRD measurement result confirmed that the prepared nanoparticles exhibit a hexagonal wurtzite structure. The plots of intensity versus 2θ angle were drawn using the origin software. The xrd pattern of the nanoparticles is shown in Fig. 5.1. As we see from Fig. 5.1, the nanoparticles showed crystalline nature with 2θ peaks lying at 31.76, 34.38, 36.12, 47.42, 56.66, 62.74, 66.44, 67.96, 69.2, 72.5, 77.04, 81.38 and 89.56 corresponding to the lattice planes (100), (002), (101), (102), (110), (103), (200), (112), (201), (004), (202), (104) and (203), respectively. The peaks are sharp and intense which reveals that the particles have good crystalline nature with minimum noise distortion or impurities. These peak positions coincide with ICSD-26170 for ZnO nanoparticle powder, a hexagonal wurtzite structure with lattice parameters,

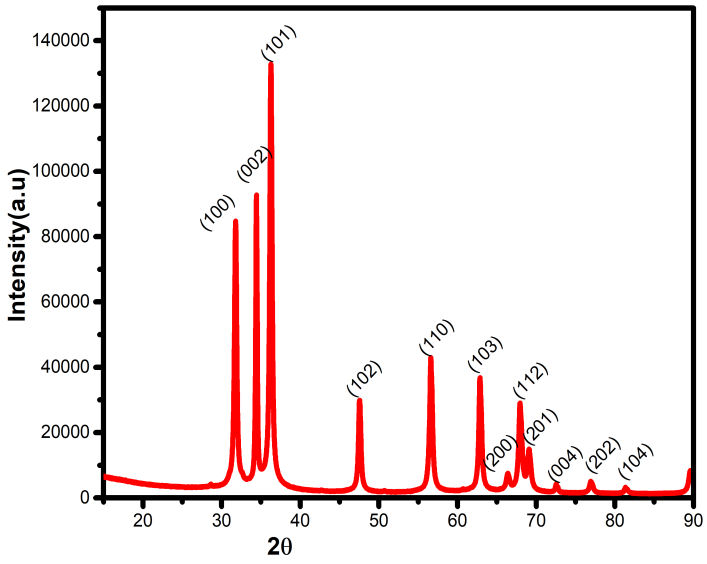

Figure 5.1: XRD pattern of ZnO NPs.

$a = 0.324986\ nm$ and $c = 0.520662\ nm$ and its space group: P63mc as it is evidently shown in Fig. 5.2. X'Pert High Score Plus software has been used to evaluate the alignment of peaks of the measured XRD spectra with peaks of ICSD-26170 for ZnO nanoparticle powder. From Fig. 5.2, the green peaks are the peaks of ICSD-26170 for ZnO nanoparticle powder and the black peaks are the XRD spectra of our sample. Similar x-ray diffraction patterns were reported by [88].

The crystallite size (D) of the samples were obtained from the XRD data using Debyee-Scherrer formula given by

$$D = \frac{\kappa\lambda}{\beta cos\theta}. \tag{5.1.1}$$

Where D is the crystallite size, κ is the shape factor which depends on the particle's shape. We set $\kappa = 0.9$ and λ is the $Cu\kappa_{\alpha 1}$ radiations ($\lambda = 0.1541\ nm$) and β is the

average full width at half maximum (FWHM) of all peaks of the XRD measurement in radians.

θ is the Bragg angle taken from 2θ value corresponding to all peaks of the XRD pattern measured in radians. The calculated crystallite size was 19.89 nm.

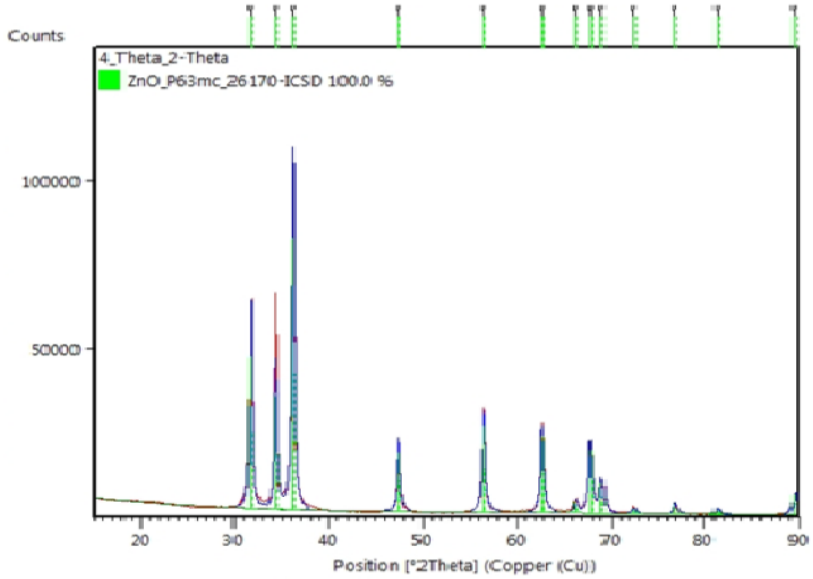

Figure 5.2: XRD Pattern of ZnO NPs and ICSD-26170 pattern for ZnO NPs(profile fitting is done Xper software.)

On account of Bragg's law, i.e.,

$$2d \sin\theta = n\lambda \tag{5.1.2}$$

where n refers the order of diffraction and d refers the interplaner distance between two diffracting planes [89]. For hexagonal crystal with lattice parameters a and c, the

interplaner distance d can be described in terms of Miller indices (hkl) as

$$\frac{1}{d_{hkl}^2} = \frac{4}{3}\left(\frac{h^2 + hk + k^2}{a^2}\right) + \frac{l^2}{c^2} \tag{5.1.3}$$

For the first order approximation (diffraction order $n = 1$), Eq. (5.1.2) will be reduced to

$$2d\sin\theta = \lambda \tag{5.1.4}$$

For the (100) orientation, Eq. (5.1.3) will be reduced to

$$\frac{1}{d_{hkl}^2} = \frac{4}{3a^2} \tag{5.1.5}$$

Again for (002) orientation, Eq. (5.1.3) becomes

$$\frac{1}{d_{hkl}^2} = \frac{4}{c^2} \tag{5.1.6}$$

On account Eqs. 5.1.4, 5.1.5 and 5.1.6, we can get,

$$a = \frac{\lambda}{\sqrt{3}\sin\theta} \tag{5.1.7}$$

and

$$c = \frac{\lambda}{\sin\theta}. \tag{5.1.8}$$

By feeding our XRD data in to Eqs. (5.1.7) and (5.1.8), we determined the lattice parameters a, c and their ratio as $a = 0.3250677\ nm$, $c = 0.5212783\ nm$ and $\frac{c}{a} = 1.604$. These lattice parameters are approximated to the results $a = 0.326\ nm$, $c = 0.5188\ nm$ which are reported by [90]. By inserting the lattice parameters a and c values in to Eq. (5.1.3), we determined the interplaner spacing d at (002) orientation to be $d = 0.261\ nm$. The cell volume of our wurtzite hexagonal ZnO NPs sample was determined by

$$V = \frac{3\sqrt{3}}{2}a^2c. \tag{5.1.9}$$

Based on this equation and the above values of the parameters, the cell volume was obtained to be $V = 0.1431\ nm^3$.

The dislocation density (δ), the length of the dislocation lines per unit volume of the crystal, designates the amount of defects in the sample and it can be calculated by

$$\delta = \frac{1}{D^2}. \tag{5.1.10}$$

Here D is the crystal size and since $D = 19.89\ nm$, δ becomes $2.52810^{-4}\ nm^{-2}$

The bond length between Zn and O (Zn-O) can be obtained by

$$L = \sqrt{\left(\frac{a^2}{3} + \left(\frac{1}{2} - u\right)^2 c^2\right)}. \tag{5.1.11}$$

Here a and c are the lattice parameters where as u is the positional parameter in the hexagonal wurtzite structure. It measures the magnitude by which each atom is displaced with respect to the neighboring one along the c axis and it can be expressed in terms of the lattice parameters as follow:

$$u = \frac{a^2}{3c^2} + \frac{1}{4}. \tag{5.1.12}$$

The parameter u is inversely related with the c/a ratio in such a way to maintain the four tetrahedral dimensions remain approximately constant due to the distortion of tetrahedral angles. By substituting the values of a and c, we obtained that $u = 0.3796$. This result is almost equal to the results $u = 0.3783$ which is reported by [91]. On the other hand, the value of L obtained ($L = 0.19789\ nm$) is nearly equal to the ($L = 0.19767\ nm$) which is reported by [92].

5.1.2 Estimation of Microstrains (ε)

We used Williamson-Hall (W-H) methods particularly, Uniform deformation model (UDM) method in order to determine the microstrain of ZnO NPs sample. According to Williamson and Hall, in the XRD diffraction, line broadening β_T of the peaks is due to the combination effect of the crystallites size β_D and microsrain β_ε. That is, the total broadening is given by

$$\beta_T = \beta_D + \beta_\varepsilon. \tag{5.1.13}$$

Here β_D is the FWHM (broadening of the peaks) in radians which can be determined by taking the average value of the Gaussian multiple fit of the peaks of the XRD data and β_ε which is caused by the strain are given by Eqs. (5.1.14) and (5.15), respectively.

$$\beta_D = \frac{\kappa\lambda}{D\cos\theta} \tag{5.1.14}$$

$$\beta_\varepsilon = 4\varepsilon\tan\theta \tag{5.1.15}$$

Substituting Eqs. (5.14) and (5.15) into Eq. (5.1.13) gives

$$\beta_T = \frac{\kappa\lambda}{D\cos\theta} + 4\varepsilon\tan\theta \tag{5.1.16}$$

Multiplying both side of Eq. (5.1.16) by $\cos\theta$ results

$$\beta_T\cos\theta = \frac{\kappa\lambda}{D} + 4\varepsilon\sin\theta \tag{5.1.17}$$

This equation is known as Williamson-Hall equation. It represents the uniform deformation model (UDM). In this model, the strain is taken as uniform in all crystallographic directions and the crystal is considered as isotropic. Moreover, the properties of the material are independent of the direction via which the measurement is taken.

$\beta_T \cos\theta_{hkl}$ versus $4\sin\theta_{hkl}$ were plotted and from the linear fit of the data, both the strain and the crystal size were determined. That is the slope of the plot and the y intercept stand for the strain ε and $\frac{\kappa\lambda}{D}$ respectively. Accordingly, the strain ε and the average crystal size D were obtained to be $\varepsilon = 0.0509$ and $D = 19.584\ nm$. The value of the crystal size $D = 19.584\ nm$ is almost equal to the value of the crystal size obtained by Debye-Sheerer method, $D = 19.891\ nm$.

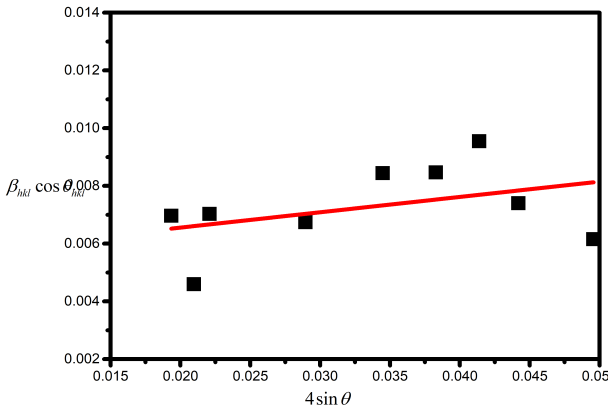

Figure 5.3: Plot of$\beta_T \cos\theta_{hkl}$ versus $4\sin\theta_{hkl}$.

5.1.3 SEM Analysis

The morphological features of the synthesized ZnO nanoparticle was studied by Scanning Electron Microscope and the images of powder sample is depicted in Fig. 5.4. The powder consists of a combination of particles with no specific shapes, platelets with small pores, Needle-like shapes and flowers-like shapes.

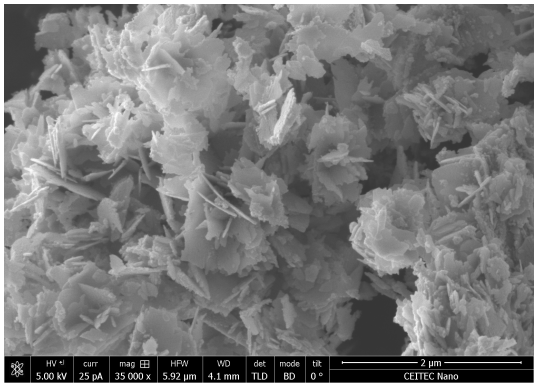

Figure 5.4: SEM Image of ZnO NPs.

5.1.4 UV/Vis Absorption Spectrum Analysis

The optical absorption spectrum of the nanoparticle was recorded at visible and ultra-violet region by Ocean Optics Spectrophotometers (JAZ -3-chanel) and its absorbance versus wavelength graph is shown in Fig. 5.5. This graph is quite similar to the graph reported by [93].

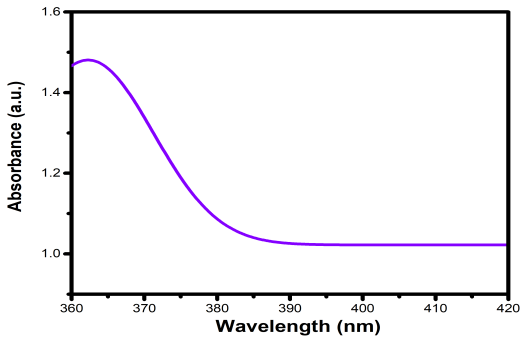

Figure 5.5: UV-Vis absorption spectrum of ZnO nanoparticles.

As it is observed from Fig. 5.5, the absorbance peak is 362.39 nm which is lower than

the absorbance peak of bulk ZnO (388 nm) [88], which denotes that there is a blue shift in the spectrum with respect to the bulk ZnO. This in turn indicates that the band gap of the ZnO nanoparticles is larger than the corresponding bulk zinc oxide. It may be due to a quantum confinement effect [94]. This absorption is due to the transition of electrons from the top of the valance band to the bottom the conduction band. ZnO nanoparticle is a direct band gap semiconductor material and therefore, the energy band gap was determined by Taucs plot.

According to Tauc-Mott relation,

$$(\alpha h\nu)^n = B(h\nu - E_g), \tag{5.1.18}$$

where $h\nu$ is the incident energy, B is energy independent constant, and α is the absorption coefficient associated with the strong absorption region of the sample which can be calculated from absorbance (A) and the path length (l) of the sample. Also, n represents the nature of transition and its value depends on the type the transition, i.e., it has the value 2 for direct transition and 1/2 for an indirect transition. Since ZnO NP is a direct band gap semiconductor, we take $n = 2$. The Tauc's plot is a plot we took the energy, $(\alpha h\nu)^2$ versus $h\nu$. The point where the tangent line touches the $h\nu$-axis represents the band gap energy which in case is found to $Eg = 3.29\ eV$. Our result, is less than the finding, $Eg = 3.5\ eV$, reported by [95]. $Eg = 3.5\ eV$ was for the whose average particle size of is 29 nm. It is clear that as the average particle size decreases, the band gap energy increases owing to Quantum size effect. So our finding is reasonable.

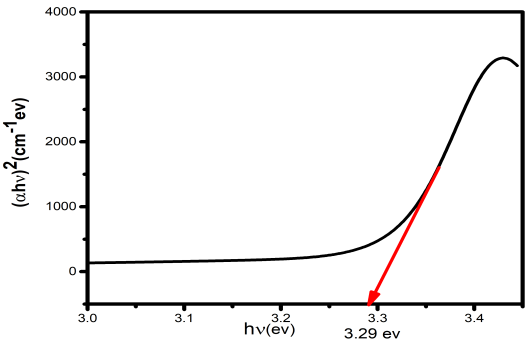

Figure 5.6: Tauc's plot of ZnO nanoparticles in the UV-Vis range.

5.1.5 FTIR Analysis

FTIR is powerful tool for probing the purities and the structure of the powders. Besides, it is used to estimate the functional groups which are embedded on the surface of the particle. The bonds which are on the surface of ZnO NPs might affect its properties. A series of absorption peaks can be found, corresponding to the vibration modes of impurities such as hydroxyl, carboxylate, carboxyl, and alkane present in the nanopowders. Fig. 6 depicts the FTIR spectra of the synthesized ZnO NPs sample. The FTIR spectra clearly revealed a strong, broad peak at $3405cm^{-1}$ which stands for $O-H$ stretching mode which indicates the existence of small amount of water absorbed by the surface of ZnO nanostructure. It may be either from the $NaOH$ which was the precursor for synthesizing the NPs or from the adsorption of atmospheric moisture. The absorption peak which is recorded at 1755 cm^{-1} will probably corresponds to the $C-O-H$ bonding. The band around 1295 cm^{-1} represents the $C-O$ stretching due to the atmospheric CO_2. The $O-H$ bending is observed at 926 cm^{-1}. The absorption peak observed at 598 cm^{-1} reveals that there

is $Zn - O$ stretching vibration.

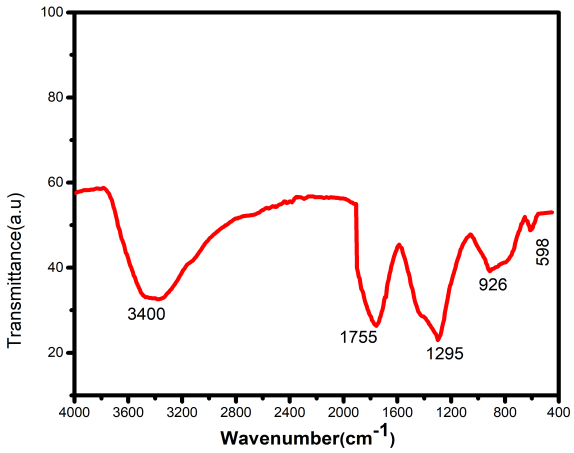

Figure 5.7: FITR spectrum of ZnO nanoparticles.

5.1.6 Photoluminescence Spectroscopy

The emission spectrum of ZnO nanopowders which are prepared by the sol-gel method from zinc acetate and sodium hydroxide is shown in Fig. 5.8. The photoluminescence (PL) spectra of the ZnO NPs exhibit emission peak on of 523 nm, over a wavelength range of 430 nm to 730 nm. This emission peak reveals the green band contribution in the emission spectra. This green band emission which is observed at 523 nm is associated with zinc interstitials and oxygen vacancies.

5.2 Fluorescence Quenching of Ferulic Acid

The peak of the fluorescence spectra of FA was observed at 350 nm. The fluorescence intensity of FA decreased with increasing ZnO NP with various concentrations. The

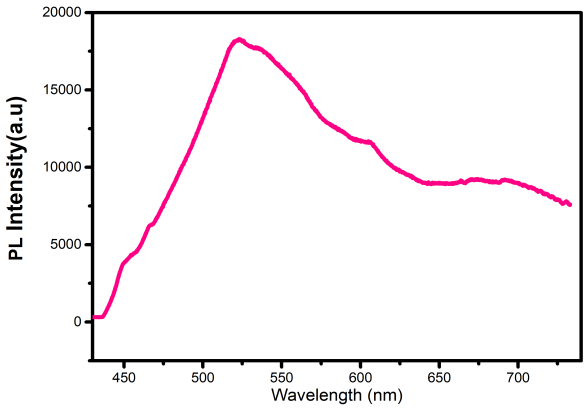

Figure 5.8: PL spectra of ZnO nanopaticles.

fluorescence spectra of FA (0.154 μ M) in the absence and presence of increasing amount of ZnO NPs (0-1.750) μ M at the temperatures of 298 K, 310 K, and 316 K are shown in Figs. 5.9, 5.10, and 5.11; respectively.

This indicated that FA was quenched with ZnO NPs. The strong quenching effects clearly indicate the existence of binding between FA and zinc oxide nanoparticles [96]. In order to interpret the quenching mechanism of the molecules, the fluorescence quenching data were analyzed according to the the Stern-Volmer equation given by: [97, 98]:

$$\frac{F_0}{F} = 1 + K_q\tau_0[Q] = 1 + K_{SV}[Q]. \tag{5.2.1}$$

Where F and F_0 are the fluorescence intensities in the presence and absence of the quencher, [Q] (the quencher concentration); K_q is the bimolecular quenching constant rate and τ_0 is the lifetime of the fluoropher in the exited state in the absence of quencher $[Q]$. The Stern-Volmer quenching constant K_{SV} value will be determined from the linear fitting of $\frac{F_0}{F}$ versus $[Q]$ plots. For static quenching, as temperature

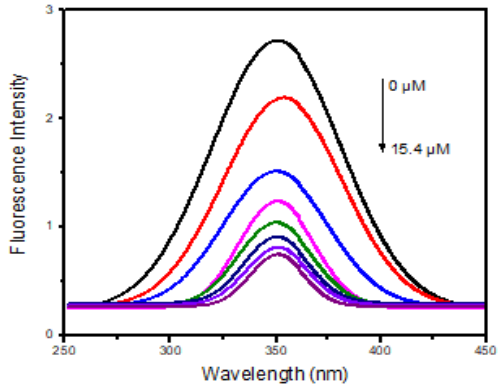

Figure 5.9: Fluorescence spectra of FA (15.4 μ M) in the absence and presence of ZnO NPs at 298 K.

increases, the bimolecular quenching constant decreases [98, 99]. But for dynamic quenching, the bimolecular quenching constant is increased with increasing temperature because a higher temperature results in a higher diffusional coefficient. Similarly, a higher temperature is also likely to result in decreases in the stability of the complex and thus lower the value of the static quenching constant [100, 101]. The Stern-Volmer quenching constant K_{SV} values at the temperatures of 298 K, 310 K, and 316 K is determined from the linear fitting of the plots of $\frac{F_0}{F}$ versus $[ZnO]$ and its values are tabulated in Table 5.1.

The plots indicated that within the given concentrations, the results displayed a good linear relationship. Table 5.1 shows that values of K_{SV} were inversely correlated with temperatures, which suggests that the fluorescence quenching of FA was initiated by the formation of ground-state complex. On the other hand, we can also determine the mechanisms of quenching from the value of bimolecular constant. The fluorescence lifetime, τ_0, of hydroxycinnamic acids was assumed to be $1 = ns$, as reported

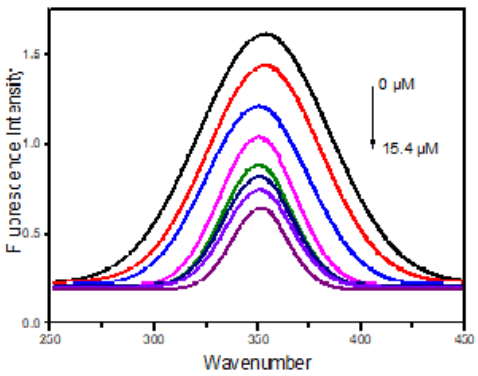

Figure 5.10: Fluorescence spectra of FA (15.4 μ M) in the absence and presence of ZnO NPs at 310 K.

Temperature in Kelvin	$K_{SV}(10^4, Lmol^{-1})$	$K_q(10^{13}, Lmol^{-1}s^{-1})$	R
298	1.55 ± 0.06	1.55 ± 0.06	0.996
310	0.88 ± 0.44	0.88 ± 0.44	0.995
316	0.66 ± 0.44	0.66 ± 0.44	0.988

Table 5.1: Stern-Volmer quenching constant K_{SV} and bimolecular binding constant K_q.

in literatures [13]. As a result

$$K_q = \frac{K_{SV}}{\tau_0}. \tag{5.2.2}$$

For dynamic quenching, the maximum scattering collision quenching constant of various quenchers is $2.0 \times 10^{10} L/mols$ [99, 96]. This revealed that the value of K_q was much greater than $2.0 \times 10^{10} L/mols$, which indicated that the probable quenching mechanism of the fluorescence of FA by ZnO NP is not caused by dynamic collision rather from the formation of a non fluorescent complex.

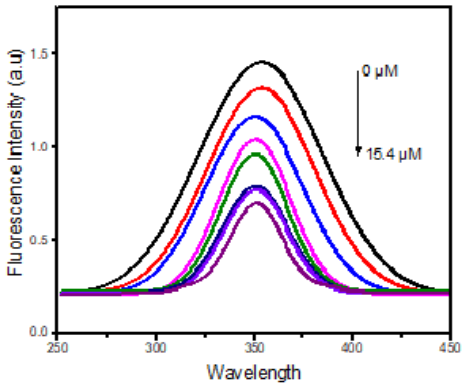

Figure 5.11: Fluorescence spectra of FA (15.4 μ M) in the absence and presence of ZnO NPs at 316 K.

5.2.1 Evaluation of the Binding Constant and Binding Site

The usefulness of drugs as therapeutic agents is basically dependent on their binding ability that can also influence the drug stability and toxicity during their chemotherapeutic process [100]. In addition, the nanoparticles molecules complex may be considered as an excellent miniature model for gaining insights into the general ferulic acid zinc oxide nanoparticles interaction. To see the binding interaction between FA and ZnO NP, the binding constant values were determined from the fluorescence intensity data. When small molecules adhere independently to the corresponding places on a macromolecule, the equilibrium between bound and free molecules will be given by the following equation:

$$\log \frac{F_0 - F}{F} = \log k + n \log [ZnO]. \tag{5.2.3}$$

Where k is the binding constant, n is the binding sites whereas F_0 , F and $[ZnO]$ are the same as Eq. (5.2.1). The plot of $\log \dfrac{F_0 - F}{F}$ versus $\log[ZnO]$ gives a straight line

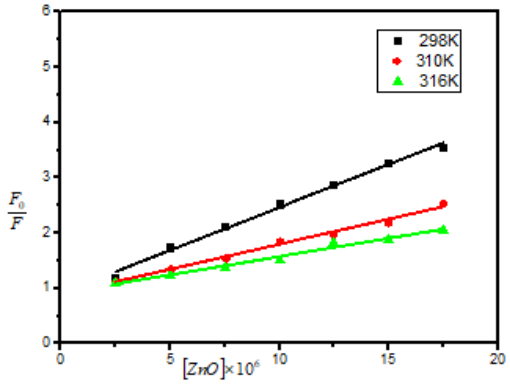

Figure 5.12: Stern-Volmer plot for FA quenching by ZnO NPs.

with slope n and y intercept log k as shown in Fig. 5.13

The binding constant is decreased with increasing temperature indicates the formation of unstable complex and partly decompose at relatively higher temperatures. Our experimental result was reasonably similar to the result reported by [102]. The values of n was found to be decreased as the temperature increases and approximately equal to 1.25 indicating that there is only one site for the binding of ZnO to FA to form the ground state complex at the three temperatures. However, Eq. (5.2.3) is not correct theoretically for the approximated value of n, it is correct only for n equal to 1. As we have found that our experimental data fit Eq. (5.2.3) with n almost equal to 1. Therefore, our experimental data can be fruitfully analyzed on the basis of Eq. (5.2.3) with n equal to 1. The obtained binding site of zinc oxide nanoparticles with FA is quite reasonable and comparable with [103, 104] findings.

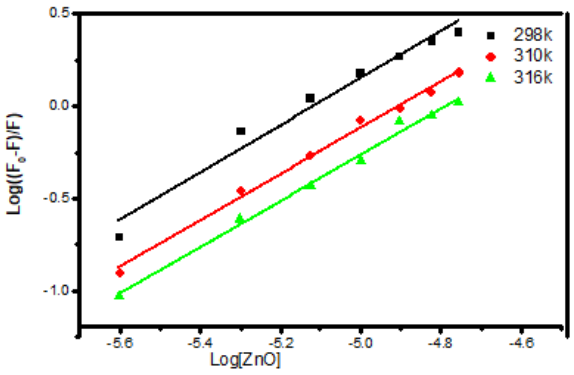

Figure 5.13: The Binding Constant of the FA - ZnO NPs.

Temp in Kelvin	Binding cons k	Binding number n	R
298	$10^{6.5}$	1.281	0.983
310	$10^{6.15}$	1.253	0.996
316	$10^{5.98}$	1.249	0.995

Table 5.2: Binding constant k and binding number n for FA-ZnO NPs interaction.

5.2.2 Thermodynamic Parameters and Binding Forces.

The interaction that exists between a small organic molecule and nanoparticles is governed by either hydrogen bonding, hydrophobic interactions, Van der Waals forces or electrostatic interactions. Ross and Subramanian have qualified the magnitudes and signs of the thermodynamic parameters those associated with various kinds of interaction that may be taken place in such association process. That is, if $\Delta H > 0$ and $\Delta S > 0$, the interaction force is hydrophobic interaction. If $\Delta H < 0$ and $\Delta S < 0$, hydrogen-bonding and Van der Waals interactions take major roles in the reaction. Electrostatic forces are more important when $\Delta H < 0$ and $\Delta S > 0$. If there is a little change in temperature, the enthalpy change (ΔH) may be taken as a constant.

In order to find clear in formation about the above concepts, the implications of the present result have been discussed in conjunction with thermodynamic characteristics obtained for ferulic acid zinc oxide nanoparticles binding, and from the Van't Hoff's equation given by

$$\ln k = \frac{\Delta H}{RT} + \frac{\Delta S}{R} \tag{5.2.4}$$

Here k and R are binding and gas constants, respectively. The enthalpy change ΔH can be determined from the slop of the Van't Hoff's relationship whereas ΔS is calculated srom the y intercept of the Van't Hoff's relationship. The free energy change, ΔG is estimated from the following equation,

$$\Delta G = \Delta H - T\Delta S \tag{5.2.5}$$

According to the binding constants at the three different temperatures, 298 K, 310 K, and 316 K, the thermodynamic parameters were determined from Van't Hoff plot (Fig. 5.14) and were presented in Table 5.3.

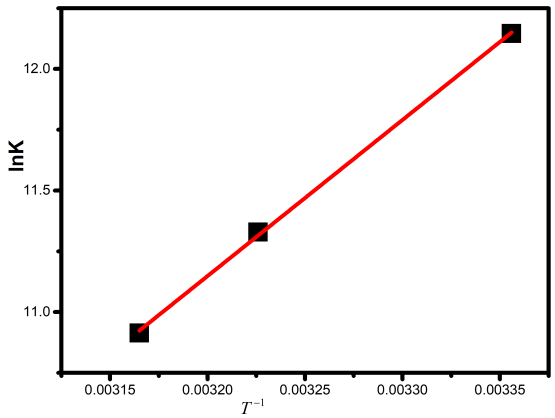

Figure 5.14: Van't Hoff plots for the binding of FA with ZnO NPs.

Temp in Kelvin	$\Delta H(kJ/mol)$	$\Delta G(kJ/mol)$	$\Delta S(J/Kmol)$	R
298	-53.301	-76.038	-76.27	0.999
310	-53.301	-76.953	-76.27	0.999
316	-53.301	-77.411	-76.27	0.999

Table 5.3: Thermodynamics parameters' values of ZnO- FA complex.

According to the values of the thermodynamic parameters (Table 5.3) for the interaction of the studied FA and ZnO NPs the binding of FA derivative to ZnO NPs is spontaneous process as indicated by the negative free energy change. Since both enthalpy and entropy changes are less than zero the binding force that exist between ferulic acid and ZnO NPs is Van der Waals and hydrogen-bonding. This binding involves the exothermic reaction as manifested by negative enthalpy change which is consistent with the decreasing k values.

5.2.3 Energy Transfer Between ZnO NPs and FA

The efficiency of energy transfer between FA and ZnO NPs can be used to evaluate the distance that exist between the donor (FA) and the acceptor (ZnO NPs) by Förster's theory of dipole-dipole energy transfer [105]. According to the Förster's theory, the efficiency of energy transfer is described by the equation [28, 106]

$$E = 1 - \frac{F_0}{F} = \frac{R_0^6}{R_0^6 + r_0^6}. \tag{5.2.6}$$

Where F_0 and F are the fluorescence emission of FA in the absence and presence of ZnO NPs respectively where as r is the distance between the acceptor and the donor and R_0 is the critical distance for 50% energy transfer [28]. R_0 Can be calculated as follow:

$$R_0^6 = 8.8 \times 10^{-25} \times k^2 \times N^{-4} \Phi J. \tag{5.2.7}$$

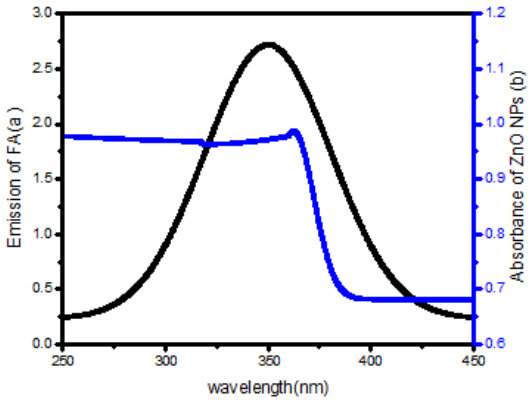

Figure 5.15: Overlap b/n the emission spectrum of FA (a) and UV absorbance spectrum of ZnO NPs (b).

Where J is the overlap integral between the donor fluorescence emission spectrum and the acceptor absorption spectrum. N is the refractive index of medium, k^2 is the spatial orientation factor of the dipole and Φ is the fluorescence quantum yield of donor. The fluorescence quantum yield Φ of FA is 0.002 [107], K^2 is 2/3 for any random orientation, the refractive index $N = 1.34$ which is the average value of the refractive indexes of water and sodium phosphate buffer solution [15]. The overlap integral between the fluorescence emission spectrum of FA and the absorption spectrum of ZnO NPs can be determined by

$$J = \frac{\int_0^\infty F(\lambda)\varepsilon(\lambda)\lambda^4 d\lambda}{\int_0^\infty F d\lambda}. \tag{5.2.8}$$

$F(\lambda)$ is the fluorescence intensity of donor in the absence of the acceptor at wavelength λ which is normalized emission spectrum (area normalized to unity) and $\varepsilon(\lambda)$ is the UV molar absorption coefficient of the acceptor at the wavelength λ. According to the above relationships and the present data, we determined the efficiency of energy

transfer E, the overlap integral J, the critical distance R_0 and the distance between the donor and the acceptor to be $E = 52.31$ %, 3.67×10^{-14} Lcm^3, $R_0 = 4.83$ nm, and $r = 4.76$ nm, respectively. The average distance between the donor (FA) and acceptor (ZnO NPs) is in the ranges of 1 and 10 nm scale, which indicates that the energy transfers from the FA to ZnO NPs occurs with high probability. In addition, the binding distance is in the range of $0.5R_0 < r < 1.5R_0$. This is one of the conditions required for applying the Förster's nonradioactive energy transfer theory.

5.3 Self-Association of Ferulic Acid

The self-association of FA was studied over the concentration range in between 8.42×10^{-5} M and 23.8×10^{-5} M . Within this range, the absorbance measurement of seven samples were carried out by circular dichroism spectrophotometer. From absorption spectra two main absorption bands that are centered at 285 nm and 311 nm were displayed. For the lowest concentration, 8.42×10^{-5} M, the absorption band at 285 nm is more intense than at 311 nm. On the other hand, as the concentration is increased from 8.42×10^{-5} M to 23.8×10^{-5} M, the absorption band at 311 nm becomes more intense than at 285 nm. Moreover, the peaks of the absorption band at 311 nm is shifted to 316 nm as shown in Fig. 5.16. Besides, the isobatic point is occurred at the wavelength $\lambda = 265$ nm. The presence of the isobatic point and the red shift of the absorbance maxima (Bathochromic shift) reveal that the FA acid molecule becomes more aggregated and gets self-association (dimerization) [108].

For numerical analysis the self-association of ferulic acid, dimer model was derived

[109] and the dimerization reaction of ferulic acid was described in the dimer model

$$M + M \overset{k_a}{\longleftrightarrow} D. \tag{5.3.1}$$

Where M and D are monomer and dimer forms of the compounds, respectively.

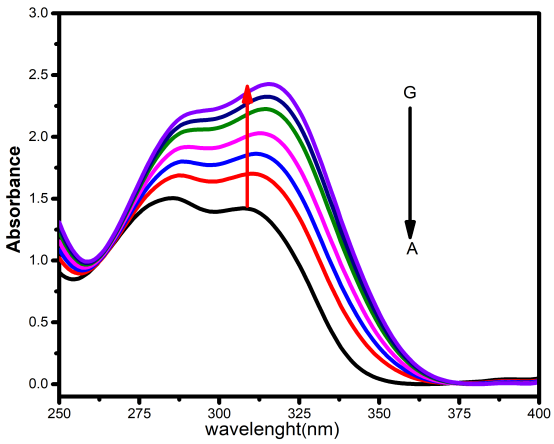

Figure 5.16: UV-Vis absorbance spectra of FA in the con range $(23.8 - 8.4) \times 10^{-5}\ M(G - A)$.

The dimerization constant K_a can be described in terms of the monomer and dimer equilibrium concentrations

$$K_a = \frac{C_D}{C_M^2}. \tag{5.3.2}$$

According to the dimer model, the mass conservation law of the overall concentration of the dissolved molecules in the solution is given by

$$C_T = C_M(1 + 2K_aC_M). \tag{5.3.3}$$

According to the dimer model, the mole fraction of the monomer and dimer at the equilibrium condition are given by

$$\alpha = \frac{C_M}{C_T}. \tag{5.3.4}$$

$$\beta = \frac{C_D}{C_T}. \tag{5.3.5}$$

On account of Eq. (5.3.3) and (5.3.4)

$$\alpha = \frac{1}{1 + 2K_a C_M}. \tag{5.3.6}$$

Solving Eq. (5.3.6) for α results

$$\alpha = \frac{-1 + \sqrt{8K_a C_T + 1}}{4K_a C_T}. \tag{5.3.7}$$

The dimer represents an important special case which will be compared with equal association constant K (EK) model stacking below [37]. There are only two solute species: monomer with mole fraction α and dimer with mole fraction β with

$$\alpha + \beta = 1 \tag{5.3.8}$$

The concentration of molecule in the dimerization system is described in terms of the mole fraction of the monomer and dimer as

$$C_T = \alpha C_M + \beta C_D \tag{5.3.9}$$

According to Beer Lambert's law, we can express the molar decadic absorption coefficient in terms of the monomer and dimer absorption coefficients as

$$\varepsilon = \alpha \varepsilon_M + \beta \varepsilon_D \tag{5.3.10}$$

Substituting Eq. (5.3.8) into Eq. (5.3.10) gives

$$\varepsilon = \alpha(\varepsilon_M - \varepsilon_D) + \varepsilon_D. \tag{5.3.11}$$

Where ε_M and ε_D are the molar decade absorption coefficient for monomer and dimer of the molecules, respectively. Substituting Eq. (5.3.7) into Eq. (5.3.11) followed by

some rearmaments yields

$$\varepsilon = \varepsilon_M + (\varepsilon_D - \varepsilon_M)\left(\frac{1-\sqrt{8k_aC_T+1}}{4K_aC_T}\right). \tag{5.3.12}$$

The unknown parameters ε_M, ε_M and K_a from Eq. (5.3.12) can be obtained by fitting this dimer model equation to the experimental data. We did this by nonlinear curve fitting applying the Levenberg-Marquardt algorithm using origin 8 software. This enabled us to find the above parameters being adjusted to attain the minimum variance between the experimental data and the theoretical value of Eq. (5.3.12). The calculated monomer ε_D and dimer extinction coefficients ε_M, and association constants K_a are 23134.44 $M^{-}cm^{-1}$, 14178 $M^{-}cm^{-1}$ and 7953 M^{-1}, respectively. These values are nearly similar to the findings of other workers in the UV/Vis region of the spectrum at room temperature for similar molecule, chlorogenic acid. The dimerization constant, the monomer and dimer extinction coefficient chlorogenic acid calculated and reported by were 1030 $M^{-}cm^{-1}$, 9580 $M^{-}cm^{-1}$ and 20500 M^{-1} [110].

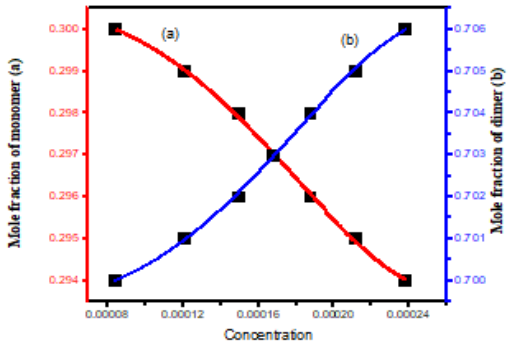

Figure 5.17: The mole fraction of monomer and dimer versus total concentratio of FA.

5.3.1 Optical properties of Ferulic Acid

Fig. 5.18 shows the UV-Vis absorption spectrum of FA in water with a concentration $7.86 \times 10^{-5}\ M$ in the wavelength regions of $250 - 400\ nm$ at room temperature. In this region FA has two isolated peaks at 285 nm, 311 nm as denoted in Fig. 5.18. The intensity of FA in water drop to zero for a wavelength greater than 357 nm.

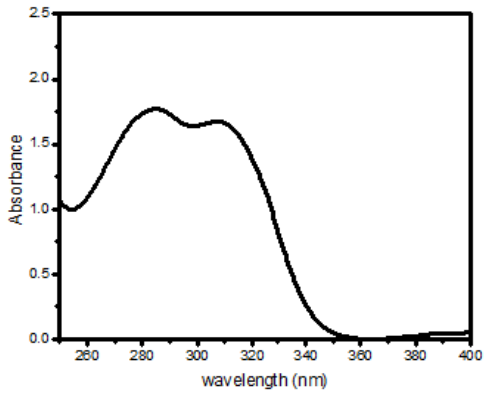

Figure 5.18: Absorbance versus wavelength graph of FA.

As we observed here the absorbance peak is recorded around 285 nm. This confirms that as the concentration becomes less than $8.42 \times 10^{-5}\ M$ there is less dimerization. The molar decadic absorption coefficient which measures an ability of the molecule to absorb the intensity of light at a given wavelength can be calculated in accordance to Eq. (3.1.54). By substituting $C = 7.86 \times 10^{-5}\ M$ and $l = 5\ mm$ into Eq. (3.1.54), the molar decadic absorption coefficient of ferulic acid at $\lambda_{max} = 285\ nm$, is found to be $\varepsilon = 21787.87\ M^{-1}cm^{-1}$. It is quite similar with, $\varepsilon = 19000 \pm 2000\ M^{-1}cm^{-1}$ which is reported by [111].

5.3.2 Integrated Absorption Cross-Section and Oscillator Strength

The integrated absorption coefficient, absorption cross-section, oscillatory strength and transition dipole moment are related to molar decadic absorption coefficient of a molecule [112]. Having taken this relation, we calculated the values for listed physical quantities of the FA. The integrated absorption coefficient α_t, the sum of the absorption coefficients over the entire band, in the frequency range ν and $d\nu$ described as

$$\alpha_t = \int \alpha d\bar{\nu}. \tag{5.3.13}$$

By taking Eqs. (3,1,54) and (3.1.55) and passing through some mathematical activities, we can find

$$\alpha = 2.303\varepsilon C. \tag{5.3.14}$$

Inserting Eq. (5.3.14) into Eq.(5.3.13), gives

$$\alpha_t = 2.303C \int \varepsilon d\bar{\nu}. \tag{5.3.15}$$

Where ε is the molar decadic absorption coefficient of ferulic acid at the concentration C.

For calculating the integrated absorption cross-section of FA, the absorbance versus wavelength graph of FA in Fig. 5.18 was recalculated into the absorption coefficient versus wavenumber as Fig. 5.19 using Origin 8 software. For convolution of the over-lapped spectra of FA and to determine the area under the peak of FA, Gaussian function was fitted to the spectra of absorption coefficient versus wavenumber, from the area under Gaussian function, the integrated absorption cross-section were calculated in water. On accoutn of Eq. (3.1.55), the absorption cross-section, a measure of the ability of a molecule to absorb photons, in the frequency range ν and $d\nu$ can

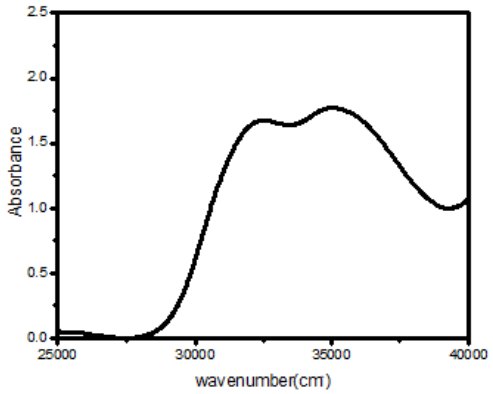

Figure 5.19: Absorbance versus wavenumber graph of Ferulic Acid

be given by

$$\sigma_t = \frac{1}{N} \int \alpha d\bar{\nu}. \tag{5.3.16}$$

Based on Eq. (5.3.13), we can have

$$\sigma_t = \frac{\alpha_t}{N}. \tag{5.3.17}$$

Where N is the number density of the molecules. It can be expressed as the product of the concentration C and Avogadro number N_A as

$$N = CN_A. \tag{5.3.18}$$

The oscillator strength expresses probability of emission or absorption which can be taken place between two states $|k\rangle$ (lower state) and $|m\rangle$ (upper state) [113]. It may be used to calculate Einstein coefficients A and B, dipole moment, transition probabilities. It is one of the fundamental quantities we need to calculate using the molar decadic absorption coefficient because it is related to the molar decadic absorption coefficient. Its value at wavelength 285 nm ia calculated in accordance to

Eq. (3.1.61) and tabulated in Table 5.4. This value indicates that the probability of emission and absorption of ferulic acid at the wavelength 285 nm is high.

5.3.3 Matrix Elements of the Transition Dipole Moment

Matrix element of the transition dipole moment denoted as $\mu_{km} = \langle \psi_k | R | \psi_m \rangle$ refers to the phenomena of transition between an initial state ψ_k and a final state ψ_m and **R** is the dipole moment operator. It is a complex vector quantity. The transition dipole moment includes the phase factors associated with the two states. Its direction is parallel to the polarization of the transition. It determines how the system will interact with an electromagnetic wave of a given polarization. The square of its magnitude gives the strength of the interaction due to transition between two states. The transition dipole moment can be described in terms of molar decadic absorption coefficient as follow

$$S = \frac{|\mu_{km}|^2}{3} \frac{\int \varepsilon d\bar{\nu}}{\bar{\nu}}. \tag{5.3.19}$$

Where S is the line shape factor and its value is $S = 2.9352 \times 10^{60}\ C^{-2} mol^{-1}$. On account of Eq. (5.3.19), the dipole moment was calculated and its values are displayed in Table 5.4. Since dipole moment $\mu_{ki} \neq 0$, the electronic transition between the initial and final states is allowed. On account of Eqs. (3.1.50) and (3.1.51) Einstein B coefficient of the transition can be calculated as

$$B_{mk} = \frac{c \ln 10}{h N_A} \frac{\int \varepsilon d\bar{\nu}}{\bar{\nu}}. \tag{5.3.20}$$

Once we obtained the Einstein B coefficient, we can obtain the Einstein A coefficient in accordance with Eq. (3.1.50).

Parameters	Values
Molar decadic absorption coefficient (ε)	$2.252 \times 10^4\ M^- cm^1$
Absorption coefficient(α)	$1.65 \times 10^4\ cm^{-2}$
Absorption cross section (σ_t)	$1.12 \times 10^{-12}\ m^2$
Oscillatory strength (f)	1.47
Transition dipole moment (μ_{km})	$4.6 \times 10^{-28}\ Cm$
Einstein B coefficient (B_{km})	$3.49 \times 10^{15}\ m^3 J^- s^{-2}$
Einstein A coefficient (A_{km})	$1.29 \times 10^{-10}\ J^- s^{-2}$

Table 5.4: Calculated Optical Properties of FA.

5.3.4 Thermodynamics Properties of Ferulic Acid

The absorbance of ferulic acid with the concentration of $9.02 \times 10^{-5}\ M$ was measured in the temperature range of $298 - 320\ K$ and the absorbance versus wavelength graph was obtained as shown in Fig. 5.20. This measurement revealed that the

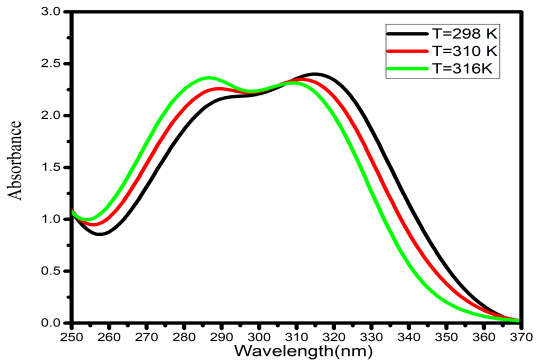

Figure 5.20: Abs FA in the temp range (298-316)K at concentration $9.02 \times 10^{-5}\ M$.

temperature has a strong impact on the absorption spectra. That is as the temperature increases the absorbance of the dimer decreased. whereas the absorbance of the monomer increases. According to the material balance equation [114, 115], the

monomer absorbance and the dimer absorbance can be related as follow.

$$\frac{A_m}{\varepsilon_m b} + \frac{A_d}{\varepsilon_d b} = C_T. \tag{5.3.21}$$

Where A_m and A_d refer the absorbance of the monomer and dimer, b is the path length and C_T is the total concentration of FA. On account of the above equation, the absorbance of the dimer A_d can be described as

$$A_d = \varepsilon_d b C_T - \frac{\varepsilon_d}{\varepsilon_m A_m}. \tag{5.3.22}$$

For the absorption measurement which is carried out on given concentration with various temperatures, we can have a series of dimer absorbance A_d and monomer absorbance A_m and from the plot of A_d versus A_m, the slope and the intercept become $\frac{\varepsilon_d}{\varepsilon_m}$ and $\varepsilon_d b C_T$, respectively. Based on this ε_m and ε_d were calculated and tabulated in Table 5.5. Moreover, the monomer- dimer equilibrium constant K_a of FA can be calculated according to Eq. (5.3.2). Based on Beer Lambert's law,

$$C_D = \frac{A_d}{\varepsilon_d b}. \tag{5.3.23}$$

$$C_M = \frac{A_m}{\varepsilon_m b}. \tag{5.3.24}$$

On account of Eqs. (5.3.2), (5.3.24) and (5.3.25)

$$K_a = \frac{\frac{A_d}{\varepsilon_d b}}{\left(\frac{A_m}{\varepsilon_m b}\right)^2}. \tag{5.3.25}$$

The values of K_a are incorporated in Table 5.5. In temperature dependence equilibrium, the thermodynamic parameters such as change free energy, change enthalpy and change entropy of the dimer ferulic acid can be determined using Van't Hoff's

Temp in Kelvin	$\varepsilon_m(M^{-1}cm^{-1})$	$\varepsilon_d(M^{-1}cm^{-1})$	$K_a(M^{-1})$
298	22527.47	13516.48	7533.158
310	22527.47	13516.48	8608.276
316	22527.47	13516.48	10169.82

Table 5.5: Monomer dimer extinction absorption coefficient and associating constant of FA in the temperature range $298 - 316\ K$.

equation. The fundamental relationship between the equilibrium constant and Gibbs energy change is given by

$$\Delta G = -RT \ln K_a. \tag{5.3.26}$$

Where R is the gas constant $R = 8.31\ Jmol^{-1}k^{-1}$ is the universal gas constant and T the temperature in Kelvin. The Gibbs energy itself is a construct of both enthalpy H and entropy S [46, 115]

$$G = H - TS \tag{5.3.27}$$

This relationship applies also to the Gibbs energy change [6]

$$\Delta G = \Delta H - T\Delta S \tag{5.3.28}$$

In accordance with the above equations, we get Van't Hoff's equation

$$\ln K_a = -\frac{\Delta H}{RT} + \frac{\Delta S}{R} \tag{5.3.29}$$

The plots of ln K_a versus T^{-1} is a straight line with slope $-\dfrac{\Delta H}{R}$ and intercept $\dfrac{\Delta S}{R}$. Therefore, the values of ΔH and ΔS were determined from the slope and the intercept, respectively. Since $\Delta H > 0$ and $\Delta S > 0$, the hydrophobic interactions are dominant for the binding of FA molecules [116, 117]. Moreover, the negative value for Gibbs free energy indicates that the absorption process of the FA is continuous. Also, the positive value of entropy confirms the increasing randomness [116]. The results are quite reasonable and comparable with the result obtained by [109, 118].

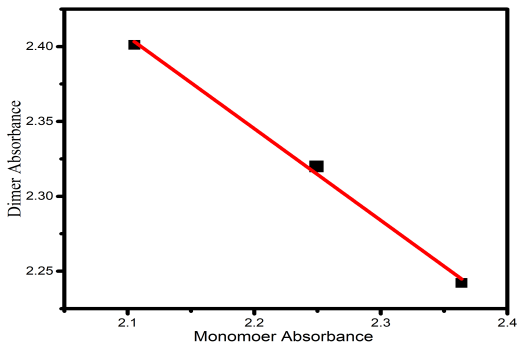

Figure 5.21: A_d vs A_m of FA in the temp range (298-316)K at con9.02×10^{-5}

Temp in Kelvin	$\Delta H(kJ/mol)$	$\Delta G(kJ/mol)$	$\Delta S(J/Kmol)$	$Regressionfactor(R)$
298	10.703	-22.084	110.02	0.981
310	10.703	-23.405	110.02	0.981
316	10.703	-24.505	110.02	0.981

Table 5.6: Thermodynamics parameters' values of FA

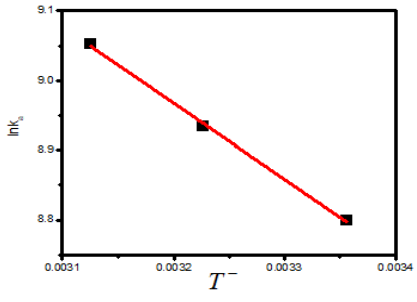

Figure 5.22: Van't Hoff's plot of FA in the temperature range $298 - 316\ K$ at concentration $9.02 \times 10^{-5}\ M$.

Chapter 6

Conclusions

This research constitutes synthesis and characterization of zinc oxide nanoparticle (ZnO NP), conjugation of ZnO NP with ferulic acid (FA), self-association properties and optical transition properties of FA. ZnO NP has been synthesized from zinc acetate and sodium hydroxide using sol-gel synthesis method and its optical and structural properties have been studied using various spectroscopic and microscopic techniques.

We analyzed XRD data by X'Pert High Score Plus software and we determined the space group, types of structure, the lattice parameters, interplaner distance, bond length, dislocation density, positional parameter and lattice planes of the synthesized nanoparticles. Using the Debby-Sheerer and William-Hall methods, we calculated the average particles size and the macro strain of the synthesized ZnO NP. From the, UV-Vis and FTIR data analysis, band gap energy and functional groups which are present on the surface of our sample have been determined. Our finding indicates that the band gap energy is 3.29 eV. FTIR data analysis confirms that the surface consists of O-H stretching, C-O-H bending, C-O stretching, O-H bending and Zn-O

stretching vibration.

ZnO NPs and FA conjugation has been investigated using fluoresces quenching method. Here, the mechanisms of quenching, Sterrn-Volmer quenching constant, bimolecular binding constant, bind number and binding site have been determined. The mechanism of quenching was obtained to be static quenching which comes from the formation of FA-ZnO NP non fluorescent complex. The thermodynamic properties such as enthalpy change entropy change and change in free energy of this complex have been determined by applying the Van't Hoff equation. The fluorescence quenching studies offered that FA is bound with ZnO NP so that the energy transfer between the FA and ZnO NP is occurred. The efficiency of energy transfer E, the overlap integral J, the critical distance R_0 and the distance between the donor and the acceptor are determined to be 52.31%, 3.67×10^{-14} Lcm^3, $R_0 = 4.83$ nm, and $r = 4.76$ nm, respectively. Dimer model was utilized to probe the self-association properties of FA. Our findings indicate that the FA molecule associates with itself by hydrophobic interaction. The calculated dimer ε_D and monomer extinction coefficients ε_M, and association constants K_a are 23134 .44 $M^{-}cm^{-1}$, 14178 $M^{-}cm^{-1}$ and 7953 M^{-1}, respectively.

The thermodynamic parameters of FA have been determined. Their value indicate that he absorption process of the FA is continuous and the randomness of solution is increasing during the absorption.

Optical transition properties of FA are also evaluated. under this section, the oscillatory strength, integrated absorption coefficient, integrated absorption cross-section dipole moment, the Einsteins A and B coefficients are investigated using integrated absorption techniques.

Bibliography

[1] Nikolai B Delone. *Basics of interaction of laser radiation with matter*. Atlantica Séguier Frontières, 1993.

[2] John Michael Brown, John M Brown, and Alan Carrington. *Rotational spectroscopy of diatomic molecules*. Cambridge University Press, 2003.

[3] Daniel C Harris and Michael D Bertolucci. *Symmetry and spectroscopy: an introduction to vibrational and electronic spectroscopy*. Courier Corporation, 1989.

[4] Matthew McCurdy, Yury Bakhirkin, Gerard Wysocki, Rafa Lewicki, and Tittel Frank. Recent advances of laser-spectroscopy-based techniques for applications in breath analysis. *Journal of breath research*, 1:014001, 2007.

[5] Florian Schmidt. *Laser-based absorption spectrometry : development of NICE-OHMS towards ultra-sensitive trace species detection*. Doctoral thesis, comprehensive summary, 2007.

[6] K Benuehll. *Fundamentals of molecular spectroscopy*. Springer, New York, 1959.

[7] Kashmira J Gohil, Shashank B Kshirsagar, and Rajkumari S Sahane. Ferulic acid-a comprehensive pharmacology of an important bioflavonoid. *Int J Pharm Sci Res*, 3:700–710, 2012.

[8] Kamila Zduńska, Agnieszka Dana, Anna Kolodziejczak, and Helena Rotsztejn. Antioxidant properties of ferulic acid and its possible application. *Skin pharmacology and physiology*, 31(6):332–336, 2018.

[9] Dongxiao Cui, Chaoqun Yan, Junqiu Miao, Xiaoyan Zhang, Jingrun Chen, Liqian Sun, Liqiang Meng, Taigang Liang, and Qingshan Li. Synthesis, characterization and antitumor properties of selenium nanoparticles coupling with ferulic acid. *Materials Science and C, Engineering*, 90:104–112, 2018.

[10] Liang-liang Shen, Hong Xu, Feng-wen Huang, Yi Li, Jie Xiao, Hua-feng Xiao, Ming Ying, Sheng-li Tian, Zhen Yang, and Gang Liu. Study on interaction of ligupurpuroside a with bovine serum albumin by multi-spectroscopic methods. *Journal of luminescence*, 154:80–88, 2014.

[11] Guang-Wei Yang, Jin-Song Jiang, and Wei-Qin Lu. Ferulic acid exerts anti-angiogenic and anti-tumor activity by targeting fibroblast growth factor receptor 1-mediated angiogenesis. *International journal of molecular sciences*, 16(10):24011–24031, 2015.

[12] VN Kalpana, V A review on green synthesis, biomedical applications, and toxicity studies of zno nps. *Bioinorganic chemistry and applications*, 2018, 2018.

[13] Reisa A Sperling and Wolfgang J Parak. Surface modification, functionalization and bioconjugation of colloidal inorganic nanoparticles. *Philosophical Transactions of the Royal Society A: Mathematical, Physical and Sciences, Engineering*, 368(1915):1333–1383, 2010.

[14] Nishima Wangoo, C Raman Suri, and G Shekhawat. Interaction of gold nanoparticles with protein: a spectroscopic study to monitor protein conformational changes. *Applied Physics Letters*, 92(13):133104, 2008.

[15] Abebe Belay, Hyung Kook Kim, and YoonHwae Hwang. Probing the interaction of caffeic acid with zno nanoparticles. *Luminescence*, 31(3):654–659, 2016.

[16] Stephen C Piscitelli. *Drug interactions in infectious diseases*. Springer, 2011.

[17] Jennifer J Kiser, James R Burton Jr, and Gregory T Everson. Drugdrug interactions during antiviral therapy for chronic hepatitis. *Nature reviews Gastroenterology and hepatology*, 10(10):596–606, 2013.

[18] Kristi M Crowe. Designing functional foods with bioactive polyphenols: Highlighting lessons learned from original plant matrices. *J. Human Nutr. and Food Sci*, 1(3):1018–1019, 2013.

[19] Ranjani Viswanatha, Sameer Sapra, B Satpati, PV Satyam, BN Dev, and DD Journal of Materials Chemistry Sarma. Understanding the quantum size effects in zno nanocrystals. 14(4):661–668, 2004.

[20] Waldo JE Beek, Martijn M Wienk, and Rene AJ Efficient hybrid solar cells from zinc oxide nanoparticles and a conjugated polymer. *Advanced Materials*, 16(12):1009–1013, 2004.

[21] T Pradeep. *NANO: The Essentials-Understanding Nanoscience and Nanotechnology.* McGraw Hill, 2007.

[22] Kerstin Koch, Bharat Bhushan, and Wilhelm Barthlott. Multifunctional plant surfaces and smart materials. In *Springer handbook of nanotechnology*, pages 1399–1436. Springer, 2010.

[23] Jin Zhong Zhang. *Optical properties and spectroscopy of nanomaterials.* World Scientific, 2009.

[24] Masataka Ohgaki, Takashi Kizuki, Mihoko Katsura, and Kimihiro Yamashita. Manipulation of selective cell adhesion and growth by surface charges of electrically polarized hydroxyapatite. 57(3):366–373, 2001.

[25] Umme Ruman, Sharida Fakurazi, Mas Jaffri Masarudin, and Mohd Zobir Hussein. Nanocarrier-based therapeutics and theranostics drug delivery systems for next generation of liver cancer nanodrug modalities. *International Journal of Nanomedicine*, 15:1437–1456, 2020.

[26] David Zinger and Nicholas E GEACiNTov. Acrylamide and molecular oxygen fluorescence quenching as a probe of solventaccessibility of aromatic fluorophores complexed with dna in relation to their conformations: Coronenedna and other complexes. *Photochemistry and photobiology*, 47(2):181–188, 1988.

[27] Gyu-Chul Yi, Chunrui Wang, and Won Il Park. Zno nanorods: synthesis, characterization and applications. *Semiconductor Science and Technology*, 20(4):22–34, 2005.

[28] Anderson Janotti and Chris G Van de Walle. Fundamentals of zinc oxide as a semiconductor. *Reports on progress in physics*, 72(12):126501, 2009.

[29] G Nagaraju, GC Shivaraju, G Banuprakash, and Dinesh Rangappa. Photocatalytic activity of zno nanoparticles: synthesis via solution combustion method. *Materials Today: Proceedings*, 4(11):11700–11705, 2017.

[30] Kwangjae Cho, XU Wang, Shuming Nie, and Dong M Shin. Therapeutic nanoparticles for drug delivery in cancer. *Clinical cancer research*, 14(5):1310–1316, 2008.

[31] Swati S Kulkarni and MD Shirsa. Optical and structural properties of zinc oxide nanoparticles. *International Journal of Advanced Research in Physical Science*, 2(1):14–18, 2015.

[32] Hadis Morkoç and Ümit Özgür. *Zinc oxide: fundamentals, materials and device technology*. John Wiley & Sons, 2008.

[33] BK Meyer, H Alves, 1, DM Hofmann, W Kriegseis, D Forster, F Bertram, J Christen, A Hoffmann, M Straßburg, M Dworzak, et al. Bound exciton and donor–acceptor pair recombinations in zno. *physica status solidi (b)*, 241(2):231–260, 2004.

[34] Zhong Lin Wang. Nanostructures of zinc oxide. *Materials today*, 7(6):26–33, 2004.

[35] Muthuchamy Maruthupandy, Muthusamy Anand, Govindhan Maduraiveeran, Santhanakrishnan Suresh, Akbar Sait Hameedha Beevi, and Radhakrishnan Jeeva Priya. Investigation on the electrical conductivity of zno

nanoparticles-decorated bacterial nanowires. *Advances in Natural Sciences: Nanoscience and Nanotechnology*, 7(4):045011, 2016.

[36] Shiyi Ou and KinChor Kwok. Ferulic acid: pharmaceutical functions, preparation and applications in foods. *Journal of the Science of Food and Agriculture*, 84(11):1261–1269, 2004.

[37] Kamila Zduska, Agnieszka Dana, Anna Kolodziejczak, and Helena Rotsztejn. Antioxidant properties of ferulic acid and its possible application. *Skin pharmacology and physiology*, 31(6):332–336, 2018.

[38] Zhixian Huang, Larry Dostal, and JP Rosazza. Mechanisms of ferulic acid conversions to vanillic acid and guaiacol by rhodotorula rubra. *Journal of Biological Chemistry*, 268(32):23954–23958, 1993.

[39] Marimuthu Srinivasan, Adluri R Sudheer, and Venugopal P Menon. Ferulic acid: therapeutic potential through its antioxidant property. *Journal of clinical biochemistry and nutrition*, 40(2):92–100, 2007.

[40] Lloyd Condict, Jasmeet Kaur, Andrew Hung, John Ashton, and Stefan Kasapis. Combined spectroscopic, molecular docking and quantum mechanics study of -casein and ferulic acid interactions following uht-like treatment. *Food Hydrocolloids*, 89:351–359, 2019.

[41] Young Taek Sohn and Jin Hee Oh. Characterization of physicochemical properties of ferulic acid. *Archives of pharmacal research*, 26(12):1002–1008, 2003.

[42] Peter W Atkins and Ronald S Friedman. *Molecular quantum mechanics*. Oxford university press, 2011.

[43] John C Lindon, George E Tranter, and David Koppenaal. *Encyclopedia of spectroscopy and spectrometry*. Academic Press, 2016.

[44] Colin N Banwell and Elaine M McCash. *Fundamentals of molecular spectroscopy*, volume 851. McGraw-Hill New York, 1994.

[45] PS Sindhu. Fundamentals of molecular spectroscopy. 2006.

[46] Wolfgang Demtrder. *Electrodynamics and Optics*. Springer Nature, 2019.

[47] Jochen Stutz and Ulrich Platt. Numerical analysis and estimation of the statistical error of differential optical absorption spectroscopy measurements with least-squares methods. *Applied Optics*, 35(30):6041–6053, 1996.

[48] Christopher Gerry, Peter Knight, and Peter L Knight. *Introductory quantum optics*. Cambridge university press, 2005.

[49] Brian Harold Bransden, Charles Jean Joachain, and Theodor J Plivier. *Physics of atoms and molecules*. Pearson education, 2003.

[50] Jürgen R Meyer-Arendt. Introduction to classical and modern optics. *itcm*, 1989.

[51] Yehuda B Band. *Light and matter: electromagnetism, optics, spectroscopy and lasers*, volume 1. John Wiley & Sons, 2006.

[52] Gale M Strasburg and Richard D Ludescher. Theory and applications of fluorescence spectroscopy in food research. *Trends in Food Science and Technology*, 6(3):69–75, 1995.

[53] Maurice R Eftink, Thomas J Selva, and Zygmunt Wasylewski. Studies of the efficiency and mechanism of fluorescence quenching reactions using acrylamide and succinimide as quenchers. *Photochemistry and photobiology*, 46(1):23–30, 1987.

[54] SV Camyshan, NP Gritsan, VV Korolev, and NM Bazhin. Quenching of the luminescence of organic compounds by oxygen in glassy matrices. *Chemical physics*, 142(1):59–68, 1990.

[55] Henk Knibbe, Dieter Rehm, and Albert Weller. Intermediates and kinetics of fluorescence quenching by electron transfer. *Berichte der Bunsengesellschaft für physikalische Chemie*, 72(2):257–263, 1968.

[56] Jakob Christensen, Lars Nrgaard, Rasmus Bro, and Sren Balling Engelsen. Multivariate autofluorescence of intact food systems. *Chemical reviews*, 106(6):1979–1994, 2006.

[57] Georges A Wagnieres, Willem M Star, and Brian C Wilson. In vivo fluorescence spectroscopy and imaging for oncological applications. *Photochemistry and photobiology*, 68(5):603–632, 1998.

[58] ENRICO Gratton, DAVID M Jameson, GREGORIO Weber, and BERNARD Alpert. A model of dynamic quenching of fluorescence in globular proteins. *Biophysical journal*, 45(4):789–794, 1984.

[59] Jihad René Albani. *Principles and applications of fluorescence spectroscopy*. John Wiley & Sons, 2008.

[60] Craig Y Okada and Martin Rechsteiner. Introduction of macromolecules into cultured mammalian cells by osmotic lysis of pinocytic vesicles. *Cell*, 29(1):33–41, 1982.

[61] Kenneth S Schmitz. *Introduction to dynamic light scattering by macromolecules*. Elsevier, 2012.

[62] Markus Grabolle, Monika Spieles, Vladimir Lesnyak, Nikolai Gaponik, Alexander Eychmuller, and Ute Resch-Genger. Determination of the fluorescence quantum yield of quantum dots: suitable procedures and achievable uncertainties. *Analytical chemistry*, 81(15):6285–6294, 2009.

[63] Demetra AC Czegan and Diana K Hoover. Uv–visible spectrometers: versatile instruments across the chemistry curriculum, 2012.

[64] Arkadii Efimovich Lutskii, Viktor Vasil'evich Prezhdo, LI Degtereva, and VG Gordienko. Spectroscopy of intermolecular field interactions in solutions. *Russian Chemical Reviews*, 51(8):802–817, 1982.

[65] Narayani Ghosh, Ramakanta Mondal, and Saptarshi Mukherjee. Inverse temperature dependence in static quenching versus calorimetric exploration: binding interaction of chloramphenicol to β-lactoglobulin. *Langmuir*, 31(29):8074–8080, 2015.

[66] Robert M Clegg. *Fluorescence resonance energy transfer and nucleic acids*, volume 211, pages 353–388. Elsevier, 1992.

[67] Paul R Selvin. The renaissance of fluorescence resonance energy transfer. *Nature structural biology*, 7(9):730–734, 2000.

[68] Kay M Parkhurst and Lawrence J Parkhurst. Kinetic studies by fluorescence resonance energy transfer employing a double-labeled oligonucleotide: hybridization to the oligonucleotide complement and to single-stranded dna. *Biochemistry*, 34(1):285–292, 1995.

[69] Pyare L Khanna and Edwin F Ullman. 4, 5-dimethoxy-6-carboxyfluorescein: a novel dipole-dipole coupled fluorescence energy transfer acceptor useful for fluorescence immunoassays. *Analytical biochemistry*, 108(1):156–161, 1980.

[70] JR Lakowicz. *Theory of Energy transfer for a donor-acceptor pair*, pages 445–448. Springer Science, Berlin, Germany, 2006.

[71] Markus Antonietti, Eckhard Wenz, Lyudmila Bronstein, and Mariana Seregina. Synthesis and characterization of noble metal colloids in block copolymer micelles. *Advanced Materials*, 7(12):1000–1005, 1995.

[72] Parvez Iqbal, Jon A Preece, and Paula M Mendes. Nanotechnology: The top-down and bottom-up approaches. *Supramolecular chemistry: from molecules to nanomaterials*, 2012.

[73] M Fernandez-Garcia, A Martinez-Arias, JC Hanson, and JA Rodriguez. Nanostructured oxides in chemistry: characterization and properties. *Chemical reviews*, 104(9):4063–4104, 2004.

[74] Ajay Vasudeo Rane, Krishnan Kanny, VK Abitha, and Sabu Thomas. *Methods for synthesis of nanoparticles and fabrication of nanocomposites*, pages 121–139. Elsevier, 2018.

[75] Harish Kumar and Renu Rani. Structural and optical characterization of zno nanoparticles synthesized by microemulsion route. *International Letters of Chemistry, Physics and Astronomy*, 14:26–36, 2013.

[76] Alain C Pierre and Gerard M Pajonk. Chemistry of aerogels and their applications. *Chemical Reviews*, 102(11):4243–4266, 2002.

[77] Gaurav Sharma, Sonika Pandey, Somenath Ghatak, Geeta Watal, and Prashant K Rai. Potential of spectroscopic techniques in the characterization of green nanomaterials. In *Nanomaterials in Plants, Algae, and Microorganisms*, pages 59–77. Elsevier, 2018.

[78] Scott A Speakman. Basics of x-ray powder diffraction. *the Center for Materials Science and Engineering at MIT, Tech. Rep. Massachusetts-USA*, 2011.

[79] TG Fawcett, SN Kabekkodu, JR Blanton, CE Crowder, and TN Blanton. simulation tools and references for the analysis of nanomaterials. *Adv. X-Ray Anal.*, 58:108–120, 2015.

[80] Orazio Svelto and David C Hanna. *Principles of lasers*, volume 1. Springer, 2010.

[81] Joseph I Goldstein, Dale E Newbury, Patrick Echlin, David C Joy, Charles Fiori, and Eric Lifshin. Electron-beam-specimen interactions. In *Scanning Electron Microscopy and X-Ray Microanalysis*, pages 53–122. Springer, 1981.

[82] Daisuke Shindo and Hiraga Kenji. *High-resolution electron microscopy for materials science*. Springer Science & Business Media, 2012.

[83] IH Campbell and Ph M Fauchet. The effects of microcrystal size and shape on the one phonon raman spectra of crystalline semiconductors. *Solid State Communications*, 58(10):739–741, 1986.

[84] Gerald D Fasman. Circular dichroism and the conformational analysis of biomolecules, 2013.

[85] PM Bayley. *The analysis of circular dichroism of biomolecules*, volume 27. Elsevier, 1973.

[86] Timothy H Gfroerer. Photoluminescence in analysis of surfaces and interfaces. *Encyclopedia of analytical chemistry: applications, theory and instrumentation*, 2006.

[87] Holger Borchert, Dirk Dorfs, Colm McGinley, Sorin Adam, Thomas Möller, Horst Weller, and Alexander Eychmüller. Photoemission study of onion like quantum dot quantum well and double quantum well nanocrystals of cds and hgs. *The Journal of Physical Chemistry B*, 107(30):7486–7491, 2003.

[88] Harish Kumar and Renu Rani. Structural and optical characterization of zno nanoparticles synthesized by microemulsion route. *International Letters of Chemistry, Physics and Astronomy*, 14:26–36, 2013.

[89] Ying Liu, Yue Liu, and Michael GB Drew. Comparison of calculations for interplanar distances in a crystal lattice. *Crystallography Reviews*, 23(4):252–301, 2017.

[90] R Raji and KG Gopchandran. Zno nanostructures with tunable visible luminescence: Effects of kinetics of chemical reduction and annealing. *Journal of Science: Advanced Materials and Devices*, 2(1):51–58, 2017.

[91] K Taha, M Mhamed, and H Idriss. Mechanical fabrication and characterization of zinc oxide (zno) nanoparticles. *J. Ovon. Res*, 11(6):271–276, 2015.

[92] Urai Seetawan, Suwit Jugsujinda, Tosawat Seetawan, Ackradate Ratchasin, Chanipat Euvananont, Chabaipon Junin, Chanchana Thanachayanont, Prasarn Chainaronk, et al. Effect of calcinations temperature on crystallography and nanoparticles in zno disk. *Mater Sci Appl*, 2(09):1302–1306, 2011.

[93] Susan Azizi, Rosfarizan Mohamad, and Mahnaz Mahdavi Shahri. Green microwave-assisted combustion synthesis of zinc oxide nanoparticles with citrullus colocynthis (l.) schrad: characterization and biomedical applications. *Molecules*, 22(2):301–314, 2017.

[94] Gopal Ramalingam, Poopathy Kathirgamanathan, Ganesan Ravi, Thangavel Elangovan, Nadarajah Manivannan, Kaviyarasu Kasinathan, et al. Quantum confinement effect of 2d nanomaterials. In *Quantum Dots-Fundamental and Applications*. IntechOpen, 2020.

[95] S Naseem Shah, S Imran Ali, S Rizwan Ali, M Naeem, Yasmeen Bibi, S Rehan Ali, S Masood Raza, Yousuf Khan, and Sikander Khan Sherwani. Synthesis and characterization of zinc oxide nanoparticles for antibacterial applications. *Journal of Basic and Applied Sciences*, 12:205–210, 2016.

[96] Ben G Yacobi. *Semiconductor materials: an introduction to basic principles*. Springer Science & Business Media, 2003.

[97] Joshua Jortner. Cluster size effects. *Zeitschrift fr Physik D Atoms, Molecules and Clusters*, 24(3):247–275, 1992.

[98] Shuji Sakohara, Masahiro Ishida, and Marc A Anderson. Visible luminescence and surface properties of nanosized zno colloids prepared by hydrolyzing zinc acetate. *The Journal of Physical Chemistry B*, 102(50):10169–10175, 1998.

[99] Johan Agrell, Gabriele Germani, Sven G Järås, and Magali Boutonnet. Production of hydrogen by partial oxidation of methanol over zno-supported palladium catalysts prepared by microemulsion technique. *Applied Catalysis A: General*, 242(2):233–245, 2003.

[100] Alan S Edelstein and RC Cammaratra. *Nanomaterials: synthesis, properties and applications*. CRC press, 1998.

[101] Klaus D Sattler. *Handbook of nanophysics: principles and methods*. CRC press, 2010.

[102] A Bhogale, N Patel, P Sarpotdar, J Mariam, PM Dongre, A Miotello, and DC Kothari. Systematic investigation on the interaction of bovine serum albumin with zno nanoparticles using fluorescence spectroscopy. *Colloids and Surfaces B: Biointerfaces*, 102:257–264, 2013.

[103] Abebe Belay, Hyung Kook Kim, and Yoon-Hwae Hwang. Spectroscopic study of binding of chlorogenic acid with the surface of zno nanoparticles. *Russian Journal of Physical Chemistry A*, 91(9):1781–1790, 2017.

[104] Gopa Mandal, Sudeshna Bhattacharya, and Tapan Ganguly. Mode of bindings of zinc oxide nanoparticles to myoglobin and horseradish peroxidase: A spectroscopic investigations. *journal of Applied Physics*, 110(2):024701, 2011.

[105] Wim H De Jong and Paul JA Borm. Drug delivery and nanoparticles: applications and hazards. *International journal of nanomedicine*, 3(2):133, 2008.

[106] Younan Xia, Peidong Yang, Yugang Sun, Yiying Wu, Brian Mayers, Byron Gates, Yadong Yin, Franklin Kim, and Haoquan Yan. One-dimensional nanostructures: synthesis, characterization, and applications. *Advanced materials*, 15(5):353–389, 2003.

[107] Urban J Wünsch, Kathleen R Murphy, and Colin A Stedmon. Corrigendum: Fluorescence quantum yields of natural organic matter and organic compounds: Implications for the fluorescence-based interpretation of organic matter composition. *Frontiers in Marine Science*, 3:9–20, 2016.

[108] R Bruce Martin. Comparisons of indefinite self-association models. *Chemical reviews*, 96(8):3043–3064, 1996.

[109] DahYu Kao, WayTai Shu, and JennShing Chen. A consistent determination of the dimerization constants of the selfassociation of 2, 2dimethyl3ethyl3pentanol in carbon tetrachloride from its infrared spectral data. *Journal of the Chinese Chemical Society*, 52(6):1171–1178, 2005.

[110] Shiyi Ou and Kin-Chor Kwok. Ferulic acid: pharmaceutical functions, preparation and applications in foods. *Journal of the Science of Food and Agriculture*, 84(11):1261–1269, 2004.

[111] Michael Kasha, HR Rawls, and M Ashraf El-Bayoumi. The exciton model in molecular spectroscopy. *Pure and Applied Chemistry*, 11(3):371–392, 1965.

[112] Aleksandrovich Davydov, Anatoli and NT Sheppard. Molecular spectroscopy of oxide catalyst surfaces, 2003.

[113] Kentaro Sekiguchi, Shoichi Yamaguchi, and Tahei T Tahara. Formation and dissociation of rhodamine 800 dimers in water: steady-state and ultrafast spectroscopic study. *he Journal of Physical Chemistry A*, 110(8):2601–2606, 2006.

[114] Hyun-Wook Ryu, Bo-Seok Park, Sheikh A Akbar, Woo-Sun Lee, Kwang-Jun Hong, Youn-Jin Seo, Dong-Charn Shin, Jin-Seong Park, and Gwang-Pyo Choi. Zno solgel derived porous film for co gas sensing. *Sensors and Chemical, Actuators*, 96(3):717–722, 2003.

[115] Gabriela CG Waschewsky, Robert Horansky, and Veronica Vaida. Effect of dimers on the temperature-dependent absorption cross section of methyl iodide. *The Journal of Physical Chemistry*, 100(28):11559–11565, 1996.

[116] Ahmed Abdur Rehman, Tarique Sarwar, Hussain Arif, Syed Saqib Ali, Haseeb Ahsan, Mohammad Tabish, and Fahim Halim Khan. Spectroscopic and thermodynamic studies on ferulic acidalpha-2-macroglobulin interaction. *Journal of Molecular Structure*, 1144:254–259, 2017.

[117] Yue Zhang, Guowen Zhang, Yu Li, and Yuting Hu. Probing the binding of insecticide permethrin to calf thymus dna by spectroscopic techniques merging with chemometrics method. *Journal of agricultural and food chemistry*, 61(11):2638–2647, 2013.

[118] Kanagalakshmi Ambothi, Rajendra Prasad Nagarajan, et al. Ferulic acid prevents ultraviolet-b radiation induced oxidative dna damage in human dermal fibroblasts. *International Journal of Nutrition, Pharmacology, Neurological Diseases*, 4(4):203–213, 2014.